A

	Amino acid sequence	Sensitivity to TRIM5α			
		AGM	CM	Hu	SPRY(-)
GH123	WMYRPQNPVP	+++	+++	++	-
GH123/A	----A-----	+++	-	+	-
GH123/Q	----Q-----	+++	-	+	-
SIVmac239	WMYRQQNPIP	+++	+	-	-
SIVmac239/P	----P-----	+++	++	+	-

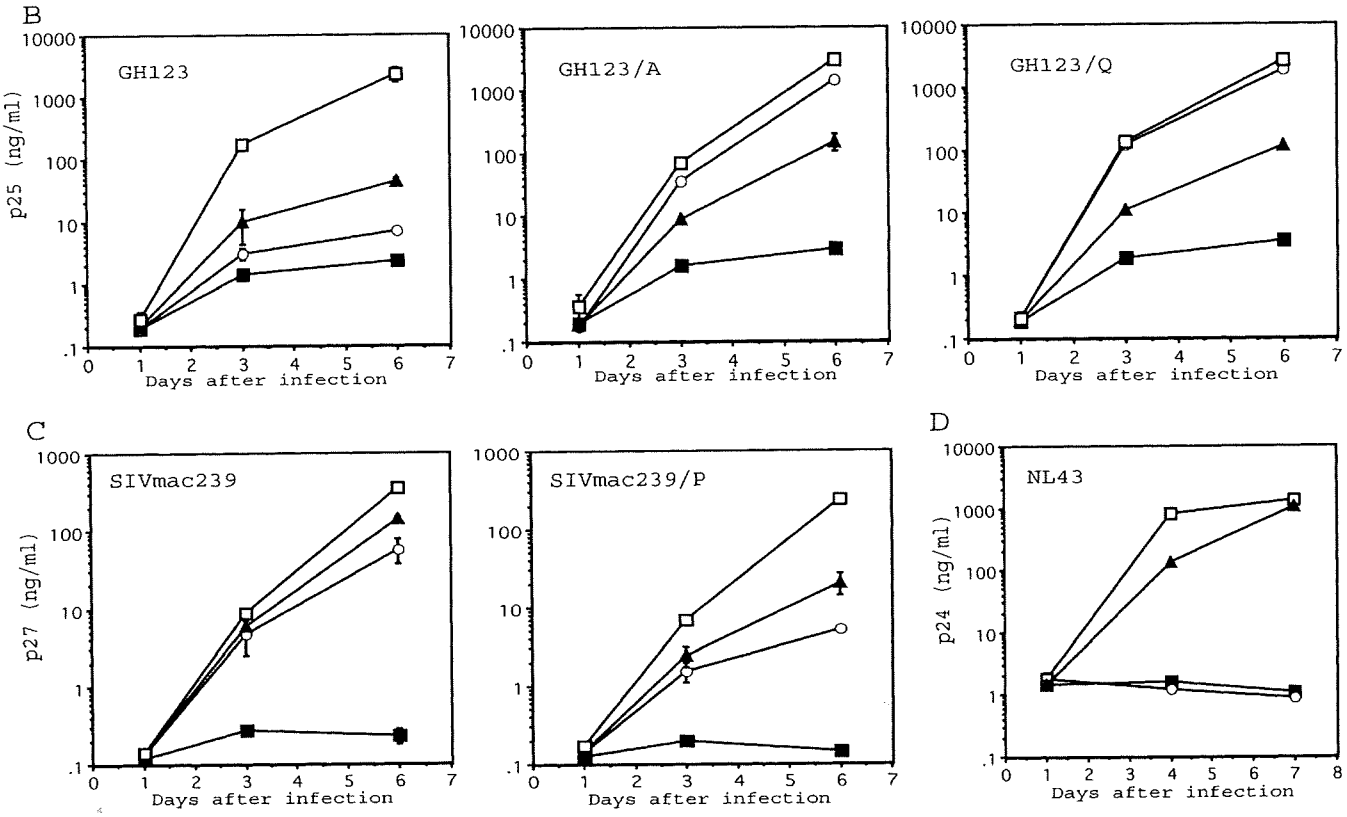

FIG. 3. (A) Mutant GH123/A and GH123/Q viruses generated by changing a single amino acid of proline to alanine or glutamine and mutant SIVmac239/P virus generated by changing a single amino acid of glutamine to proline by site-directed mutagenesis. Dashes indicate the unmutated amino acid residues. +++, ++, +, and − denote more-than-300-fold, 40- to 100-fold, 6- to 40-fold, and less-than-2.5-fold suppression of virus growth, respectively, compared with what was seen for the negative control at day 6 in the presence of the various TRIM5αs indicated. (B to D) MT4 cells were infected with CM-TRIM5α-SeV (open circles), Hu-TRIM5α-SeV (filled triangles), AGM-TRIM5α-SeV (filled squares), or CM-SPRY(−)-SeV (open squares). Nine hours after infection, cells were inoculated with GH123, mutant GH123/A, or GH123/Q viruses (panel B), with SIVmac239 or mutant SIVmac239/P virus (panel C), or with HIV-1 NL43 virus (panel D). Culture supernatants were periodically assayed for levels of virus CA. Error bars show actual fluctuations between measurements of CA in duplicate samples. A representative of three independent experiments is shown.

determined the nucleotide sequences of PCR-amplified DNA fragments corresponding to proviral DNA encoding the CAs of the HIV-2 isolates. Figure 2A shows the deduced amino acid sequences of the HIV-2 CAs. TRIM5α-sensitive GH123 and UC12 had proline at the 120th (GH123) or corresponding 119th (UC12) position, while the other six TRIM5α-resistant isolates showed alanine (UC1 and UC14) or glutamine (UC2, UC7, 9429, and 12741) at the corresponding 119th position. Except for this substitution, there was no substitution observed commonly and specifically for GH123 and UC12.

To determine whether the single amino acid at the 119th or 120th position of the HIV-2 CA affects the virus's susceptibility to CM and Hu TRIM5α, we constructed two mutant GH123 viruses carrying either alanine (GH123/A) or glutamine (GH123/Q) at the 120th position (Fig. 3A). As shown in Fig. 3B, all three viruses grew substantially and to similar titers in CM-SPRY(−)-SeV-infected MT4 cells. In CM-TRIM5α-SeV-infected cells, both GH123/A and GH123/Q grew to titers more than 250 times higher than those of the wild-type GH123. In the Hu-TRIM5α-SeV-infected cells, both mutant viruses grew to titers approximately fourfold higher than those of the wild type (Fig. 3B). In contrast, replication of the three viruses could not be detected in the AGM-TRIM5α-SeV-infected cells (Fig. 3B). Unlike CM TRIM5α, AGM TRIM5α pos-

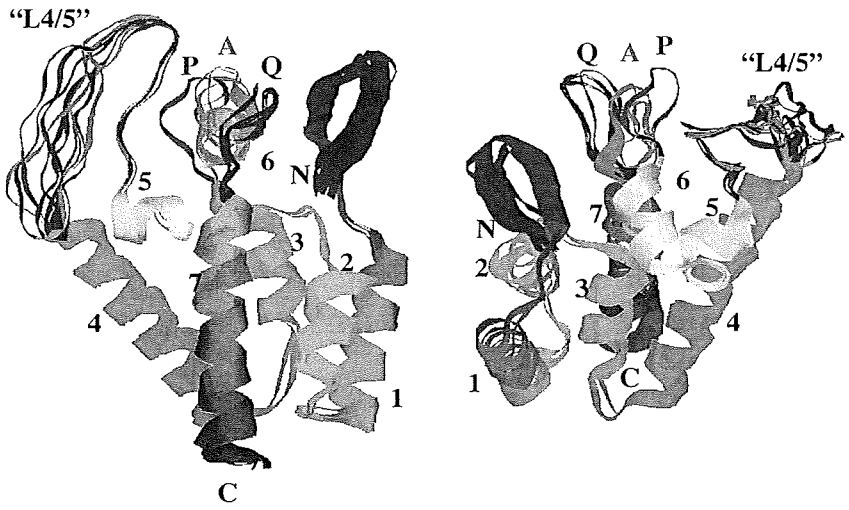

FIG. 4. Structural model of the N-terminal halves of HIV-2 CAs. The 3-D models of 10 HIV-2 CAs were constructed with the homology-modeling technique using "MOE-Align" and "MOE-Homology" in the Molecular Operating Environment (MOE) as described previously (18, 19). Superimposition of the 10 HIV-2 models showed that the overall 3-D structures of the N-terminal domains of the variants are very similar. N and C indicate the amino termini and carboxyl termini, respectively. The ribbons represent the backbones of HIV-2 CAs, and the seven color-coded α-helices are labeled. P, A, and Q indicate L6/7 with a proline residue (GH123 and UC12 [in red]), an alanine residue (UC1, UC14, and GH123/A [in green]), and a glutamine residue (UC2, UC7, 9429, 12741, and GH123/Q [in blue]), respectively, at the 120th position. L4/5 is labeled with a color scheme the same as that for L6/7. The presence of proline residues conferred a sensitive phenotype; alanine and glutamine conferred phenotypes resistant to restriction by CM TRIM5α. Models from two different angles are shown.

sessed a potent antiviral activity against SIVmac as well as HIV-1 and HIV-2 (26, 27). These results indicate that the single amino acid at the 120th position of the GH123 CA indeed affects susceptibility to the restriction of virus replication by CM TRIM5α.

There is more than 87% amino acid identity in CA between HIV-2 GH123 and SIVmac239. SIVmac239 is resistant to CM TRIM5α (26) and contains glutamine at the 118th position, which corresponds to the 120th position of the GH123 CA. To determine whether this particular amino acid also affects the resistance of SIVmac239 to CM TRIM5α, we constructed a mutant SIVmav239 carrying a proline at the 118th position (SIVmac239/P) (Fig. 3A). As shown in Fig. 3C, both wild-type and mutant SIVmac239 grew substantially and to similar titers in the CM-SPRY(−)-SeV-infected MT4 cells. In CM-TRIM5α-SeV-infected cells, the mutant SIVmac239 grew to titers that were approximately 10 times lower than those of the wild type. The glutamine-to-proline mutation also caused an approximately eightfold decrease in the virus titer in Hu-TRIM5α-SeV-infected cells (Fig. 3C). In contrast, neither virus grew in AGM-TRIM5α-SeV-infected cells (Fig. 3C). These results indicate that the glutamine at the 118th position of the SIVmac239 CA also affects resistance to the CM and Hu TRIM5αs.

Nineteen HIV-2 and 20 SIVsmm or SIVmac CA sequences were listed in the Los Alamos sequence database (Fig. 2B). All SIV isolates except for SMM-SL92B carried glutamine at the position corresponding to the 120th position of GH123 (Fig. 2B). SMM-SL92B, which carries alanine, was most distantly related to all the other HIV-2 and SIV isolates from the phylogenetic analysis (data not shown). These results suggest that all SIV isolates are resistant to CM and Hu TRIM5αs. In contrast, HIV-2 group A isolates showed a mixture of proline, alanine, and glutamine and HIV-2 group B isolates had a mixture of proline and alanine in the CA (Fig. 2B). Other HIV-2 isolates also carried proline and glutamine, with H2AB-7312A, which had glycine, being the only exception (Fig. 2B). These results suggest that different HIV-2 isolates have diverse susceptibilities to CM and Hu TRIM5αs. It is likely that glutamine-to-alanine or glutamine-to-proline substitutions occurred after the proposed zoonotic transfer of virus from monkeys to humans (11).

To obtain structural insight into the mechanisms by which this amino acid change in the CA alters viral susceptibility to restriction by TRIM5α, three-dimensional (3-D) models of HIV-2 CAs were constructed with the homology-modeling technique based on the crystal structure of the HIV-1 CA N-terminal domain (15). These models consist of those with proline (GH123, UC12), alanine (UC1, UC14, GH123/A), and glutamine (UC2, UC7, 9429, 12741, GH123/Q) at the 120th position. The thermodynamically optimized 3-D structures showed that the HIV-2 CA N-terminal domains consist of a packed core structure from which seven α-helices and three loops protrude, which is basically the same conformation as that of their HIV-1 counterparts (15) (Fig. 4).

The 120th amino acid that affects the viral susceptibility to TRIM5α restriction is located in the loop between helices 6 and 7 (L6/7) (Fig. 4, labeled Q, A, P). Especially worth noting is that the amino acid substitution at the 120th position is predicted to induce marked changes in the configuration of L6/7. The loop with the TRIM5α-sensitive proline (GH123 and UC12, Fig. 4, labeled P) is positioned most closely to the loop between helices 4 and 5 (L4/5). We obtained results the same as those described above when we constructed HIV-2 CA models based on the HIV-1 CA structure in solution (data not shown) (8). In HIV-1, L4/5 interacts directly with cyclophilin A (15, 24, 36). It is possible that TRIM5α recognizes the partic-

ular structure formed by two closely aligned L4/5 and L6/7 with proline.

Previously, a single amino acid substitution at the 110th position of N-MLV CA was shown to determine viral susceptibility to Fv1 (20), another type of restriction factor in mice (2), as well as to Hu TRIM5α (14, 31, 37). The fact that the amino acids at analogous positions of both N-MLV and HIV-2 CAs (25, 36) affected sensitivity to Hu and CM TRIM5αs, respectively, suggested that N-MLV and HIV-2 are recognized by TRIM5α in a similar manner. It would be interesting to investigate whether the 120th position of HIV-2 CA affects its sensitivity to TRIM5α of other OWM cells.

Human TRIM5α has no or very little effect on HIV-1 or SIVmac infection (30, 32, 34, 35, 38). Unlike HIV-1 (Fig. 3D), HIV-2 isolates sensitive to CM TRIM5α were slightly more sensitive to Hu TRIM5α than those resistant to CM TRIM5α (Fig. 1 and 3B). As shown in Fig. 4, half of the HIV-2 isolates in the database carried proline, which would be sensitive to Hu TRIM5α. This finding may be one of the reasons why HIV-2 is less pathogenic than HIV-1 (9). Since certain HIV-2 patients with high plasma HIV-2 loads developed AIDS as rapidly as HIV-1 patients (10), examining the effect of sensitivity to Hu TRIM5α of HIV-2 strains in infected individuals on the rate of disease progression merits attention.

We thank J. Sakuragi and S. Sakuragi for helpful discussions and S. Bandou and N. Teramoto for assistance.

This work was supported by grants from the Ministry of Education, Culture, Sports, Science, and Technology and the Ministry of Health, Labor and Welfare, Japan.

REFERENCES

1. **Barnett, S. W., K. K. Murthy, B. G. Herndier, and J. A. Levy.** 1994. An AIDS-like condition induced in baboons by HIV-2. Science **266**:642–646.
2. **Best, S., P. Le Tissier, G. Towers, and J. P. Stoye.** 1996. Positional cloning of the mouse retrovirus restriction gene Fv1. Nature **382**:826–829.
3. **Castro, B. A., S. W. Barnett, L. A. Evans, J. Moreau, K. Odehouri, and J. A. Levy.** 1990. Biologic heterogeneity of human immunodeficiency virus type 2 (HIV-2) strains. Virology **178**:527–534.
4. **Castro, B. A., M. Nepomuceno, N. W. Lerche, J. W. Eichberg, and J. A. Levy.** 1991. Persistent infection of baboons and rhesus monkeys with different strains of HIV-2. Virology **184**:219–226.
5. **Evans, L. A., J. Moreau, K. Odehouri, H. Legg, A. Barboza, C. Cheng-Mayer, and J. A. Levy.** 1988. Characterization of a noncytopathic HIV-2 strain with unusual effects on CD4 expression. Science **240**:1522–1525.
6. **Evans, L. A., J. Moreau, K. Odehouri, D. Seto, G. Thomson-Honnebier, H. Legg, A. Barboza, C. Cheng-Mayer, and J. A. Levy.** 1988. Simultaneous isolation of HIV-1 and HIV-2 from an AIDS patient. Lancet **ii**:1389–1391.
7. **Fujita, M., A. Yoshida, A. Sakurai, J. Tatsuki, F. Ueno, H. Akari, and A. Adachi.** 2003. Susceptibility of HVS-immortalized lymphocytic HSC-F cells to various strains and mutants of HIV/SIV. Int. J. Mol. Med. **11**:641–644.
8. **Gitti, R. K., B. M. Lee, J. Walker, M. F. Summers, S. Yoo, and W. I. Sundquist.** 1996. Structure of the amino-terminal core domain of the HIV-1 capsid protein. Science **273**:231–235.
9. **Gottlieb, G. S., S. E. Hawes, H. D. Agne, J. E. Stern, C. W. Critchlow, N. B. Kiviat, and P. S. Sow.** 2006. Lower levels of HIV RNA in semen in HIV-2 compared with HIV-1 infection: implications for differences in transmission. AIDS **20**:895–900.
10. **Gottlieb, G. S., P. S. Sow, S. E. Hawes, I. Ndoye, M. Redman, A. M. Coll-Seck, M. A. Faye-Niang, A. Diop, J. M. Kuypers, C. W. Critchlow, R. Respess, J. I. Mullins, and N. B. Kiviat.** 2002. Equal plasma viral loads predict a similar rate of CD4+ T cell decline in human immunodeficiency virus (HIV) type 1- and HIV-2-infected individuals from Senegal, West Africa. J. Infect. Dis. **185**:905–914.
11. **Hahn, B. H., G. M. Shaw, K. M. De Cock, and P. M. Sharp.** 2000. AIDS as a zoonosis: scientific and public health implications. Science **287**:607–614.
12. **Hasegawa, A., H. Tsujimoto, N. Maki, K. Ishikawa, T. Miura, M. Fukasawa, K. Miki, and M. Hayami.** 1989. Genomic divergence of HIV-2 from Ghana. AIDS Res. Hum. Retrovir. **5**:593–604.
13. **Hatziioannou, T., S. Cowan, U. K. Von Schwedler, W. I. Sundquist, and P. D. Bieniasz.** 2004. Species-specific tropism determinants in the human immunodeficiency virus type 1 capsid. J. Virol. **78**:6005–6012.
14. **Hatziioannou, T., D. Perez-Caballero, A. Yang, S. Cowan, and P. D. Bieniasz.** 2004. Retrovirus resistance factors Ref1 and Lv1 are species-specific variants of TRIM5alpha. Proc. Natl. Acad. Sci. USA **101**:10774–10779.
15. **Howard, B. R., F. F. Vajdos, S. Li, W. I. Sundquist, and C. P. Hill.** 2003. Structural insights into the catalytic mechanism of cyclophilin A. Nat. Struct. Biol. **10**:475–481.
16. **Keckesova, Z., L. M. Ylinen, and G. J. Towers.** 2004. The human and African green monkey TRIM5alpha genes encode Ref1 and Lv1 retroviral restriction factor activities. Proc. Natl. Acad. Sci. USA **101**:10780–10785.
17. **Kestler, H., T. Kodama, D. Ringler, M. Marthas, N. Pedersen, A. Lackner, D. Regier, P. Sehgal, M. Daniel, N. King, et al.** 1990. Induction of AIDS in rhesus monkeys by molecularly cloned simian immunodeficiency virus. Science **248**:1109–1112.
18. **Kinomoto, M., R. Appiah-Opong, J. A. Brandful, M. Yokoyama, N. Nii-Trebi, E. Ugly-Kwame, H. Sato, D. Ofori-Adjei, T. Kurata, F. Barre-Sinoussi, T. Sata, and K. Tokunaga.** 2005. HIV-1 proteases from drug-naive West African patients are differentially less susceptible to protease inhibitors. Clin. Infect. Dis. **41**:243–251.
19. **Kinomoto, M., M. Yokoyama, H. Sato, A. Kojima, T. Kurata, K. Ikuta, T. Sata, and K. Tokunaga.** 2005. Amino acid 36 in the human immunodeficiency virus type 1 gp41 ectodomain controls fusogenic activity: implications for the molecular mechanism of viral escape from a fusion inhibitor. J. Virol. **79**:5996–6004.
20. **Kozak, C. A., and A. Chakraborti.** 1996. Single amino acid changes in the murine leukemia virus capsid protein gene define the target of Fv1 resistance. Virology **225**:300–305.
21. **Locher, C. P., S. W. Barnett, B. G. Herndier, D. J. Blackbourn, G. Reyes-Teran, K. K. Murthy, K. M. Brasky, G. B. Hubbard, T. A. Reinhart, A. T. Haase, and J. A. Levy.** 1998. Human immunodeficiency virus-2 infection in baboons is an animal model for human immunodeficiency virus pathogenesis in humans. Arch. Pathol. Lab. Med. **122**:523–533.
22. **Locher, C. P., D. J. Blackbourn, B. G. Herndier, G. Reyes-Teran, S. W. Barnett, K. K. Murthy, and J. A. Levy.** 1998. Transient virus infection and pathogenesis of a new HIV type 2 isolate, UC12, in baboons. AIDS Res. Hum. Retrovir. **14**:79–82.
23. **Locher, C. P., S. A. Witt, B. G. Herndier, N. W. Abbey, K. Tenner-Racz, P. Racz, N. B. Kiviat, K. K. Murthy, K. Brasky, M. Leland, and J. A. Levy.** 2003. Increased virus replication and virulence after serial passage of human immunodeficiency virus type 2 in baboons. J. Virol. **77**:77–83.
24. **Luban, J., K. L. Bossolt, E. K. Franke, G. V. Kalpana, and S. P. Goff.** 1993. Human immunodeficiency virus type 1 Gag protein binds to cyclophilins A and B. Cell **73**:1067–1078.
25. **Mortuza, G. B., L. F. Haire, A. Stevens, S. J. Smerdon, J. P. Stoye, and I. A. Taylor.** 2004. High-resolution structure of a retroviral capsid hexameric amino-terminal domain. Nature **431**:481–485.
26. **Nakayama, E. E., H. Miyoshi, Y. Nagai, and T. Shioda.** 2005. A specific region of 37 amino acid residues in the SPRY (B30.2) domain of African green monkey TRIM5alpha determines species-specific restriction of simian immunodeficiency virus SIVmac infection. J. Virol. **79**:8870–8877.
27. **Ohkura, S., M. W. Yap, T. Sheldon, and J. P. Stoye.** 2006. All three variable regions of the TRIM5alpha B30.2 domain can contribute to the specificity of retrovirus restriction. J. Virol. **80**:8554–8565.
28. **Owens, C. M., B. Song, M. J. Perron, P. C. Yang, M. Stremlau, and J. Sodroski.** 2004. Binding and susceptibility to postentry restriction factors in monkey cells are specified by distinct regions of the human immunodeficiency virus type 1 capsid. J. Virol. **78**:5423–5437.
29. **Owens, C. M., P. C. Yang, H. Gottlinger, and J. Sodroski.** 2003. Human and simian immunodeficiency virus capsid proteins are major viral determinants of early, postentry replication blocks in simian cells. J. Virol. **77**:726–731.
30. **Perez-Caballero, D., T. Hatziioannou, A. Yang, S. Cowan, and P. D. Bieniasz.** 2005. Human tripartite motif 5α domains responsible for retrovirus restriction activity and specificity. J. Virol. **79**:8969–8978.
31. **Perron, M. J., M. Stremlau, B. Song, W. Ulm, R. C. Mulligan, and J. Sodroski.** 2004. TRIM5alpha mediates the postentry block to N-tropic murine leukemia viruses in human cells. Proc. Natl. Acad. Sci. USA **101**:11827–11832.
32. **Sawyer, S. L., L. I. Wu, M. Emerman, and H. S. Malik.** 2005. Positive selection of primate TRIM5alpha identifies a critical species-specific retroviral restriction domain. Proc. Natl. Acad. Sci. USA **102**:2832–2837.
33. **Shibata, R., T. Miura, M. Hayami, K. Ogawa, H. Sakai, T. Kiyomasu, A. Ishimoto, and A. Adachi.** 1990. Mutational analysis of the human immunodeficiency virus type 2 (HIV-2) genome in relation to HIV-1 and simian immunodeficiency virus SIV (AGM). J. Virol. **64**:742–747.
34. **Stremlau, M., C. M. Owens, M. J. Perron, M. Kiessling, P. Autissier, and J. Sodroski.** 2004. The cytoplasmic body component TRIM5alpha restricts HIV-1 infection in Old World monkeys. Nature **427**:848–853.
35. **Stremlau, M., M. Perron, S. Welikala, and J. Sodroski.** 2005. Species-specific variation in the B30.2(SPRY) domain of TRIM5α determines the potency of human immunodeficiency virus restriction. J. Virol. **79**:3139–3145.
36. **Towers, G. J., T. Hatziioannou, S. Cowan, S. P. Goff, J. Luban, and P. D.**

Bieniasz. 2003. Cyclophilin A modulates the sensitivity of HIV-1 to host restriction factors. Nat. Med. **9**:1138–1143.
37. **Yap, M. W., S. Nisole, C. Lynch, and J. P. Stoye.** 2004. Trim5alpha protein restricts both HIV-1 and murine leukemia virus. Proc. Natl. Acad. Sci. USA **101**:10786–10791.
38. **Yap, M. W., S. Nisole, and J. P. Stoye.** 2005. A single amino acid change in the SPRY domain of human Trim5alpha leads to HIV-1 restriction. Curr. Biol. **15**:73–78.
39. **Ylinen, L. M., Z. Keckesova, S. J. Wilson, S. Ranasinghe, and G. J. Towers.** 2005. Differential restriction of human immunodeficiency virus type 2 and simian immunodeficiency virus SIVmac by TRIM5α alleles. J. Virol. **79**: 11580–11587.

JOURNAL OF VIROLOGY, Aug. 2007, p. 7985–7992 Vol. 81, No. 15
0022-538X/07/$08.00+0 doi:10.1128/JVI.00429-07

Minimal Region Sufficient for Genome Dimerization in the Human Immunodeficiency Virus Type 1 Virion and Its Potential Roles in the Early Stages of Viral Replication[▽]

Jun-ichi Sakuragi,* Sayuri Sakuragi, and Tatsuo Shioda

Department of Viral Infections, Research Institute for Microbial Diseases, Osaka University, Osaka, Japan

Received 28 February 2007/Accepted 11 May 2007

It has been suggested that the dimer initiation site/dimer linkage sequence (DIS/DLS) region of the human immunodeficiency virus type 1 (HIV-1) RNA genome plays an important role at various stages of the viral life cycle. Recently we found that the duplication of the DIS/DLS region on viral RNA caused the production of partially monomeric RNAs in virions, indicating that this region indeed mediates RNA-RNA interaction. In this report, we followed up on this finding to identify the necessary and sufficient region for RNA dimerization in the virion of HIV-1. The region thus identified was 144 bases in length, extending from the junction of R/U5 and U5/L stem-loops to the end of SL4. The *trans*-acting responsive element, polyadenylation signal, primer binding site, upper stem-loop of U5/L, and SL2 were not needed for the function of this region. The insertion of this region into the ectopic location of the viral genome did not affect the level of virion production by transfection. However, the resultant virions contained monomerized genomes and showed drastic reductions in infectivity. A reduction was observed especially in the reverse transcription process. An attempt to generate a replication-competent virus with monomerized genome was performed by the long-term culture of mutant virus-infected cells. All recovered viruses were wild-type revertants, indicating a fatal defect of the mutation. These results suggest that genome dimerization or DIS/DLS itself also plays an important role in the early stages of virus infection.

The retrovirus genome is a single-stranded, positive-sense RNA. The viral genome always occurs as a dimer in virus particles, and the interaction is noncovalent since heating easily dissociates purified dimeric genomes into monomers. Template strand switching between two genomes during reverse transcription is often observed in the retroviral life cycle (15). It is likely that the presence of two genomes in one virion helps the virus survive by providing an extra template that can be used when one RNA molecule is damaged and/or providing genetic variety for the progeny. However, this may not fully explain why the virion has to carry two identical RNAs in spite of severe space limitation, so the precise nature of retroviral genome dimerization is still unclear.

The identification of *cis*-acting signals for retrovirus genome dimerization was initially attempted in an in vitro assay (10, 11, 21, 34, 36). Synthesized 5′ RNA fragments of a viral genome, with a length of several hundred to a thousand bases, were found to be dimerized by heating and cooling under suitable buffering conditions. The proposed dimer initiation site/dimer linkage sequence (DIS/DLS) region of human immunodeficiency virus type 1 (HIV-1) is located within the untranslated region between the long terminal repeat (LTR) and the *gag* gene (11, 22). As these regions overlap with a packaging signal, however, it was difficult to perform mutational analysis to study the dimerization of the genome within the virion. Therefore, we recently developed a system to assess the dimerization signal operating within the HIV-1 virion without affecting the packaging ability of the genome (41). This system is an application of our previous finding that duplication of the encapsidation/dimerization signal (E/DLS) region on one RNA genome resulted in the appearance of a monomeric genome in the HIV-1 virion (40). We speculated that an additional E/DLS region at the ectopic position binds to the authentic E/DLS region on the same RNA molecules, thus competitively interfering with intermolecular dimer formation (Fig. 1A). Mutational analysis could thus be utilized to map the DIS/DLS precisely on the HIV-1 RNA. By applying this system, part of the 5′ untranscribed region (UTR) of the HIV-1 genome was examined, and separate functional maps for dimerization and encapsidation signals could be created. By comparing these two maps, we concluded that RNA dimer linkage formation must be an essential process in genome packaging, which consists of multiple sequential steps (41). In the study reported here, we employed our original system to identify the region which is necessary and sufficient for HIV-1 genome dimerization in the virion. We also report on our further investigation of the roles of the dimerization signal at various stages of viral replication and discuss the possibility that it may perform functions other than genome packaging in the viral life cycle.

MATERIALS AND METHODS

DNA constructs. The replication-competent HIV-1 proviral clone pNL4-3 (2) and pMSMBA (23), a derivative of pNL4-3, were used as progenitors for the mutant constructs described here. Mutant plasmids were constructed with standard methods. To construct pDDNT4, pDDNU4, and pDDNL4, three pairs of primers were first used for PCR amplification of the HIV-1 leader region by using the plasmid pGEM-MM (40) as a template. The first pair comprised the sense primer TarF (5′-GGTCTCTCTGGTTAGACCAG-3′) and the antisense primer SL4Rs (5′-GACGCTCTCGCACCCATC-3′), the second pair consisted of the sense primer R/U5F (5′-CACTGCTTAAGCCTCAACGATCG-3′) and the antisense primer SL4Rs, and the third pair consisted of the sense primer

* Corresponding author. Mailing address: Department of Viral Infections, Research Institute for Microbial Diseases, Osaka University, 3-1 Yamadaoka, Suita City, Osaka 565-0871, Japan. Phone: 81-6-6879-834. Fax: 81-6-6879-8347. E-mail: sakuragi@biken.osaka-u.ac.jp.

▽ Published ahead of print on 15 May 2007.

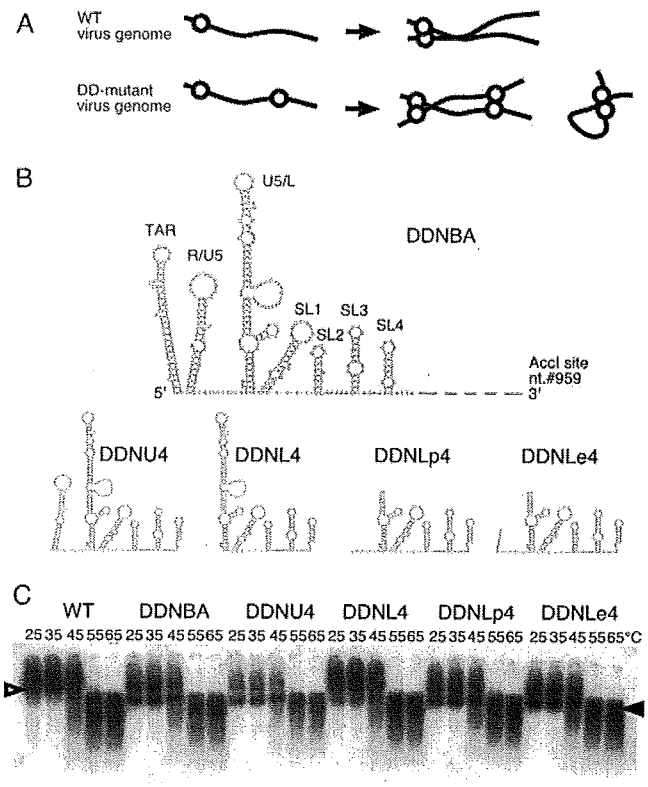

FIG. 1. The 5′ and 3′ ends of a functional domain of DLS. (A) A schematic image of monomer formation of the E/DLS duplicated mutant (DD-mutant) genome. Genomes of the WT virus form dimers, whereas those of DD-mutant form both dimers and monomers. Solid lines and open circles represent viral genome RNA and E/DLS, respectively. (B) Possible two-dimensional folds of the inserted fragment of each of the constructed mutants. nt., nucleotide. (C) Virion RNA profiles in native agarose gel. Viruses were prepared by transfection of 293T cells with pNLNh (WT) or its derivative mutants. At 48 h posttransfection, culture supernatants were harvested. Virions in the supernatant were collected by ultracentrifugation through a 20% sucrose cushion for isolation of the virion RNA. Open and solid arrowheads denote positions of dimers and monomers, respectively.

U5/LF (5′-TCTGTTGTGTGACTCTGGTAAC-3′) and the antisense primer SL4Rs. The three amplified fragments were isolated and ligated in pGEM-Teasy (Promega, Madison, WI) to generate pGEMT4sub, pGEMU4sub, and pGEML4sub, respectively. The digestion of these plasmids with EcoRI, blunt ended by T4 DNA polymerase, resulted in the isolation of approximately 300-bp fragments, including the 5′ leader region of HIV-1. These fragments were then ligated into the T4 DNA polymerase-treated NheI site of pNL4-3 to construct pDDNT4, pDDNU4, and pDDNL4, respectively. The orientation of the inserted fragments was verified by sequencing. pDDNLp4 and pDDNLe4 were constructed in a similar way, except for the use of pdLA3 (39) as a PCR template and different sense primers. The sense primer for pDDNLp4 was A3F+N (5′-TGTGCCCGTCTGTTGTGTGACTC-3′), and that for pDDNLe4 was A3U5endN (5′-AGTAGTGTGTGCCCGTCTGTTGTGTGACTC-3′). To construct pDDNLp4Δ1 and pDDNLp4Δ3, pdM and pdX (25) were used as templates for PCR amplification with the sense primer LpLA3 (5′-TGTGCCCGTCTGTTGTGTGACTCTGGTGCCAGAGGAG-3′) and the antisense primer SL4Rs, respectively. The two amplified fragments were isolated and ligated in pGEM-Teasy to generate pGEMLp4Δ1sub and pGEMLp4Δ3sub, respectively. To construct pDDNLp4Δ2, two-step PCR amplification was performed by using pGEMLp4sub as a template. The first pair of primers comprised the sense primer A3F+N and the antisense primer dS2R (5′-CAAAATTTTTGCCCCTCGCC-3′), and the second pair comprised the sense primer dS2F (5′-GGCGAGGGGCAAAAATTTTG-3′) and the antisense primer SL4Rs. Two amplified fragments were isolated, mixed, and used for the second PCR with primers A3F+N and SL4Rs to generate a mutated fragment. This fragment was then isolated and ligated in pGEM-Teasy to generate pGEMLp4Δ2sub. To construct pDDNLp4Δ4, pGEMLp4sub was used as a template for PCR amplification with the sense primer A3F+N and the antisense primer dS4 (5′-CATCTCTCCTTCTAGCC-3′). The amplified fragment was isolated and ligated in pGEM-Teasy to generate pGEMLp4Δ4sub. The digestion of pGEMLp4Δ1sub, -Δ2sub, -Δ3sub, and -Δ4sub with EcoRI, blunt ended by T4 DNA polymerase, resulted in the isolation of fragments, including the 5′ leader region of HIV-1. These fragments were then ligated into the T4 DNA polymerase-treated NheI site of pNL4-3 to construct pDDNLp4Δ1, -Δ2, -Δ3, and -Δ4, respectively. The EcoRI fragment from pGEMLp4Δ2sub (fragment Lp4Δ2) was blunt ended by T4 DNA polymerase and ligated into the BsaBI site of pDDNLp4Δ2 to create pDTNLp4Δ2. The plasmid p5′ssβglob (24) features a deletion on the 5′ untranslated region of pMSMBA (nucleotides 694 to 783) and an insertion at the point of deletion of a portion of the sequence spanning the 5′ splicing signal of the first intron of the β-globin gene. The 2.2-kb StuI-XhoI fragments containing env regions of pDDNLp4Δ2 and pDTNLp4Δ2 were inserted into the corresponding position of p5′ssβglob to create pssNLp4Δ2 and psTNLp4Δ2, respectively. The fragment Lp4Δ2 was blunt ended by T4 DNA polymerase and ligated into the T4 DNA polymerase-treated XhoI site of pNL4-3 to construct pDDXE+. The fragment Lp4Δ2 was ligated into the EcoRI site of pNL4-3 to construct pDDEE+. pDDEE+ was digested with Sse8387I, and NheI, a 4.4-kb, *pol-env* region-containing fragment, was isolated and exchanged at the same position of pDDXE+ to construct pDTEXE+. The construction of the HIV-2 *env* expression vector, pCGH2env, has been described previously elsewhere (28).

DNA transfection. 293T cells (13) (approximately 3×10^6) were seeded on dishes (diameter, 100 mm) the day before transfection with plasmid DNA (5 μg) by means of the calcium phosphate precipitation method (3). The day after transfection, the supernatant was replaced with fresh medium.

Virus infection. At 48 to 72 h posttransfection, the medium was centrifuged and the supernatant was used for infection with inoculation of equal amounts of CA-p24 into MT-4, M8166, or M8166/H1Luc cells (27). The supernatants of MT-4 or M8166 were harvested every 3 or 4 days for the multiple replication assay, while 10 μl of each cell supernatant was analyzed with the exogenous reverse transcriptase (RT) assay as described previously (43). M8166/H1Luc cells contain integrated reporter DNA carrying the HIV-1 LTR and luciferase. Upon infection with HIV-1, the HIV-1 LTR is activated along with the expression of viral transactivator Tat and luciferase expression in cytoplasm is induced. The same amount of CA-p24 recovered from each construct was inoculated into M8166/H1Luc cells, and luciferase expression within the cells was measured 24 h after infection. The luciferase assay was performed with the Bright-Glo luciferase assay system (Promega).

Isolation of RNA from virions. At 48 to 72 h posttransfection, virus particles were collected concurrently from medium as described previously elsewhere (23). The physical virus titer was determined with an enzyme-linked immunosorbent assay kit to quantitate CA-p24 (ZeptoMetrix, Inc., Buffalo, NY). To isolate RNA from particles, virions were disrupted by the addition of 1% sodium dodecyl sulfate and treated with proteinase K (300 μg/ml) at room temperature for 60 min, followed by Tris-EDTA-saturated phenol-chloroform extraction, chloroform extraction, and ethanol precipitation.

Northern blotting analysis. Pelleted RNA was resuspended in T buffer (10 mM Tris-HCl, pH 7.5, 1 mM EDTA, 1% sodium dodecyl sulfate, 100 mM NaCl, and 10% formamide), and the thermostability of dimeric viral RNA was determined by incubating RNA aliquots for 10 min at the temperatures indicated (42). RNA electrophoresis on native agarose gel and Northern hybridization analysis were performed as described previously elsewhere (41). Plasmid T7pol (42) was used to synthesize a cRNA probe for Northern hybridization. In experiments designed to assess the conversion of dimers to monomers, relative amounts of both RNA species were quantitated by PhosphorImager analysis (Fujifilm Co., Tokyo, Japan) and ratios of dimers and monomers were determined.

RNase protection assay. The antisense probe ($\sim 10^8$ cpm/mg) specific to the NL4-3 *gag* region was synthesized by in vitro transcription. One-fifth of the virion-associated RNA was mixed with 8×10^4 Cerenkov counts of ^{32}P-labeled antisense riboprobe and precipitated with ethanol. RNase protection assays were performed with an RPA III RNase protection assay kit (Ambion, Inc., Austin, TX). After electrophoresis in 5% polyacrylamide-8 M urea gels, protected RNA was quantitated by PhosphorImager analysis (Fujifilm Co.).

Real-time PCR analysis. At 48 to 72 h posttransfection, culture supernatants of the transfected cells were harvested. The supernatants were treated with DNase prior to infection to eliminate plasmid DNA contamination as described previously elsewhere (20) and inoculated into 10^6 MT-4 cells. For PCR analysis, total DNA was extracted from infected cells 20 h after infection by using a GenElute mammalian genomic DNA miniprep kit (Sigma, St. Louis, MO).

TABLE 1. Packaging efficiency of the mutants analyzed[a]

Mutant or WT	Avg ± SEM
WT	1 ± 0
DDNT4	0.84 ± 0.14
DDNU4	1.61 ± 0.26
DDNL4	1.09 ± 0.10
DDNLp4	1.04 ± 0.08
DDNLe4	0.94 ± 0.09

[a] The values were calculated by dividing the quantity of viral RNA by that of CA-p24. The value of WT (NLNh) was set at 1. Values are averages of results of at least three independent experiments.

Real-time PCR was performed with an Applied Biosystems 7500 real-time PCR system to quantitate viral cDNA synthesis during infection. Primers and TaqMan probes were selected according to criteria described previously elsewhere (19), and samples (0.5 μg DNA) were subjected to 40 cycles of PCR in a 10-μl reaction mixture. A series of known amounts of plasmid DNA were amplified along with total DNA to serve as a standard in each experiment. For the quantitation of the 2-LTR from virus DNA, a 2-LTR circle junction was cloned into pGEM-Teasy plasmid (Promega) as a TA cloning fragment by PCR amplification from 2-LTR circles, with total DNA extracted from infected MT-4 cells serving as a template. Serial dilutions of this plasmid were used as a standard to determine copy numbers of 2-LTR circles in the samples in the same manner as that for the determination of other DNA copy numbers.

For integrated proviral DNA quantitation, a modification of a recently reported Alu PCR method (7, 18) was employed (28). In short, two outward-facing Alu primers that anneal within the conserved regions of the Alu repeat element were used, together with an HIV-1 LTR-specific primer (L-M667), to optimize the probability of amplifying an LTR sequence for the first round of PCR. For the second round of PCR (real-time PCR), a lambda-specific primer (Lambda T) was used as a sense primer to detect only the amplified fragments in the first round of PCR and a TaqMan probe and an antisense primer were selected from the previous set for R/U5 DNA detection (19). The resultant PCR products were diluted 100-fold and subjected to real-time PCR.

RESULTS

The 5′ and 3′ ends of a functional domain of DIS/DLS. In a previous study of ours, the minimal RNA region required for RNA dimerization in virions was identified as a fragment inserted in the *env* region of pDDNBA (41). The fragment was approximately 500 bases long, extending from the 5′ capping site to the middle of the MA gene of the viral genome with deletion of the polyadenylation signal and primer binding site (PBS). We first constructed five mutants to precisely map the 5′ and 3′ ends of the functional region of DIS/DLS (Fig. 1). The viral genome packaging efficiency of all mutants was similar to that of the wild type (WT), indicating that the mutations had little effect on packaging ability (Table 1). The viral genome from mutant DDNT4, which contains an ectopic fragment (334 bases, from the *trans*-acting responsive element [TAR] to SL4) at the *env* region, formed a monomer very similar to that of the original mutant DDNBA (monomer content was more than 40% of the total viral genome in native condition), which indicated that sequence 3′ to SL4 was not needed for mediating RNA-RNA interactions in virions (data not shown). pDDNU4 carried a fragment from the R/U5 [poly(A)] stem-loop to SL4 (277 bases), and pDDNL4 carried a fragment from the U5/L stem-loop to SL4 (222 bases). As shown in Fig. 1B, the viral genome from DDNU4 formed a monomeric RNA comparable to DDNBA (monomer content was more than 40%), whereas the viral genome from DDNL4 formed a monomeric RNA with a greatly reduced amount of monomer (<20%). These results indicate that the 5′ end of the functional region of DIS/DLS was lost from DDNL4. We therefore added 8 and 15 nucleotides of the 5′ sequences to DDNL4 to generate DDNLp4 and DDNLe4, respectively. An upper stem-loop and PBS of the U5/L region were deleted from the inserted fragment of DDNLp4 and DDNLe4 because our previous data showed that those parts were dispensable for the dimer linkage formation function (41). Both viral RNAs of DDNLp4 and DDNLe4 formed a genome with a monomeric content (>40%) comparable to that of the WT in the virion (Fig. 1B). Taken together, these findings suggest that the region from the R/U5-U5/L junction to SL4 is sufficient to produce dimeric RNA in virions.

Minimal region sufficient for RNA dimerization is 144 bases long. We then examined the involvement in dimer linkage formation of four stem-loops, SL1 (putative "DIS"), SL2 (splicing signal), SL3 (essential region of packaging signal), and SL4 (containing *gag*AUG). Four mutants, DDNLp4Δ1, DDNLp4Δ2, DDNLp4Δ3, and DDNLp4Δ4, were constructed as derivatives of DDNLp4. Each mutant contained a deletion of one of four stem-loops on the ectopic fragment of DDNLp4 (Fig. 2A). As shown in Fig. 2B, only DDNLp4Δ2 formed a monomeric genome similar to the one derived from DDNBA,

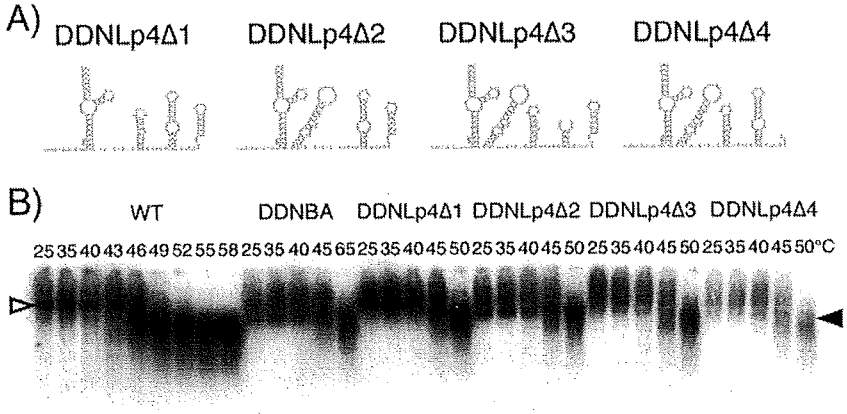

FIG. 2. Determination of the necessary and sufficient DLS in virions. (A) Probable two-dimensional folds of the inserted fragment of each of the constructed mutants. (B) Virion RNA profiles in native agarose gel. Virion RNA was isolated, and Northern hybridization was performed as described for Fig. 1. Open and solid arrowheads denote positions of dimers and monomers, respectively.

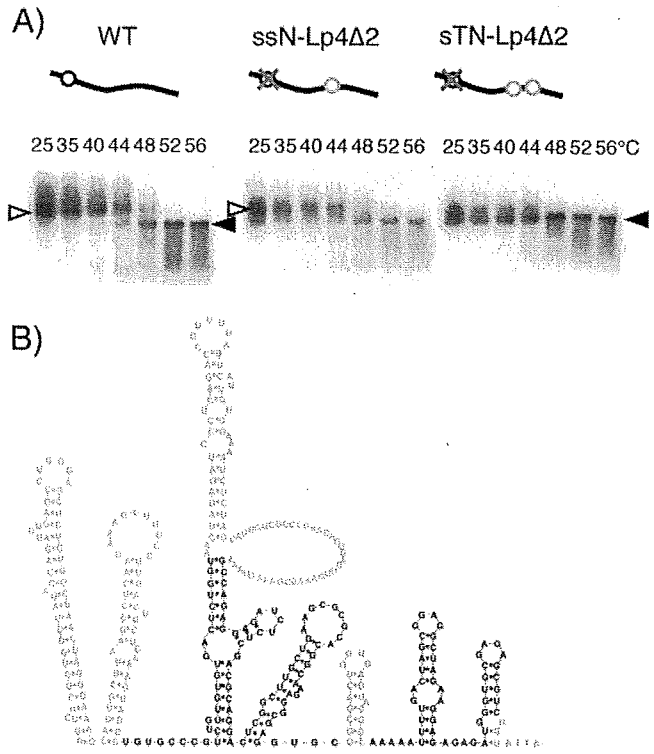

FIG. 3. Verification of the minimal DLS for its ability to induce RNA-RNA interaction in HIV-1 virions. (A) Virion RNA profiles in native agarose gel. Virion RNA was isolated, and Northern hybridization was performed as described for Fig. 1. Open and solid arrowheads denote positions of dimers and monomers, respectively. Schematic diagrams of mutants are shown above the blots. Solid lines, open circles, gray circles, and gray crosses represent viral genome RNA, authentic E/DLS, Lp4Δ2 fragments, and mutations introduced to knock out E/DLS functions, respectively. (B) A schematic Mfold representative of the verified area.

whereas other mutants displayed low levels of monomeric genome formation in virions. This indicates that the major splicing donor, SL2, is dispensable for RNA-RNA interaction, while the three other stem-loops are necessary for dimer linkage formation in virions.

In a previous study, we constructed two mutants, ssN− and sTN−, which contained a deletion of authentic DIS/DLS and an insertion of one (ssN−) or two (sTN−) DIS/DLS fragments in the ectopic position of the viral genome (39). Viral genomes from dimers formed from ssN− were similar to the WT, and nearly all viral genomes in virions of sTN− were monomers. This suggests that the two fragments inserted on one RNA strand interacted exclusively and intramolecularly with each other to prevent intermolecular dimerization. To confirm that fragment Lp4Δ2 was necessary and sufficient for RNA dimer linkage formation in virions, we constructed two mutants, ssNLp4Δ2 and sTNLp4Δ2, in the same way that ssN− and sTN− were constructed, except for the use of fragment Lp4Δ2 for insertion. As we expected, viral genomes from ssNLp4Δ2 formed dimers similar to those of the WT, while the viral genome from sTNLp4Δ2 exclusively formed monomers (Fig. 3A). Thus, the Lp4Δ2 fragment, 144 bases in length, was necessary and sufficient for mediating RNA dimerization in HIV-1 virions (Fig. 3B).

Single-round infection efficiency of HIV-1 mutant containing monomeric genome. We previously demonstrated the particle formation of HIV-1 which contained exclusively monomerized genome (39). This suggested that whole-genome dimerization is not essential for RNA packaging and particle formation of the viral genome, although dimer linkage formation of the DLS region is essential for these functions (41). On the other hand, no efficient infection or replication of HIV-1 mutants containing a monomeric genome was observed since significant reduction of intact viral DNA production occurred as a result of aberrant strand transfer and/or recombination during reverse transcription (39). Strand transfer during the reverse transcription process of the retroviral genome targets the R region of the viral LTR (12), which has also been suggested to be a hot spot for recombination (26). The production of aberrant viral cDNA products could thus be induced by the presence of multimerized R regions on the genome of the mutants. Since Lp4Δ2, the minimum DLS we identified here, did not include any R region, its ability to induce aberrant strand transfer and/or recombination by duplication of Lp4Δ2 in the viral genome was expected to be reduced. We therefore compared the single-round replication efficiencies of mutants DDNLp4Δ1, -Δ2, -Δ3, and -Δ4 pseudotyped with the HIV-2 envelope. The result demonstrated that all mutants containing Lp4 fragments showed reduced infectivity, which may be the effect of homologous recombination at a sequence-duplicated location (Fig. 4A). However, the infectivity of DDNLp4Δ2, the only mutant packaging monomeric genome, was three- to five-fold lower than that of other mutants. As the M8166/H1Luc cell assay reflects the magnitude of Tat expression of the samples, this result suggests that the mutations introduced in these constructs affect mainly the step(s) between virus penetration and early gene expression.

Reverse transcription predominantly blocked in monomeric genome mutants. To determine the step(s) in the viral replication cycle affected by the mutation described above, we analyzed the efficiency of each of the replication steps of the mutants. We chose two mutants, DDNLp4Δ2 and -Δ3, for comparison, since they are very similar in length of duplicated sequences but quite different in infectivity. We analyzed the virion production and viral RNA encapsidation ability of the mutants by purifying the virion and viral RNA from the supernatant of transfectant 293T cells. As shown in Fig. 4B, both functions of the mutants were similar or only moderately reduced compared to those of the WT, indicating that the mutations had little effect on these processes.

We next quantitated the levels of virus reverse-transcribed products, 2-LTR viral circular DNA, and integrated viral DNA using real-time PCR. HIV-2 *env*-pseudotyped virus was generated by transfection and purified, and equivalent amounts of CA-p24 were used to infect MT-4 cells. At 20 h after infection, total DNA was isolated from virus-infected cells. To examine the progress of reverse transcription, four sets of primers and probes were prepared (see Materials and Methods) and used to measure the synthesis of the strong-stop negative-strand DNA, first-strand transferred DNA, *gag* region DNA, and second-strand transferred DNA within total cellular DNA. Figure 4C shows the organized results of viral DNA quantitation.

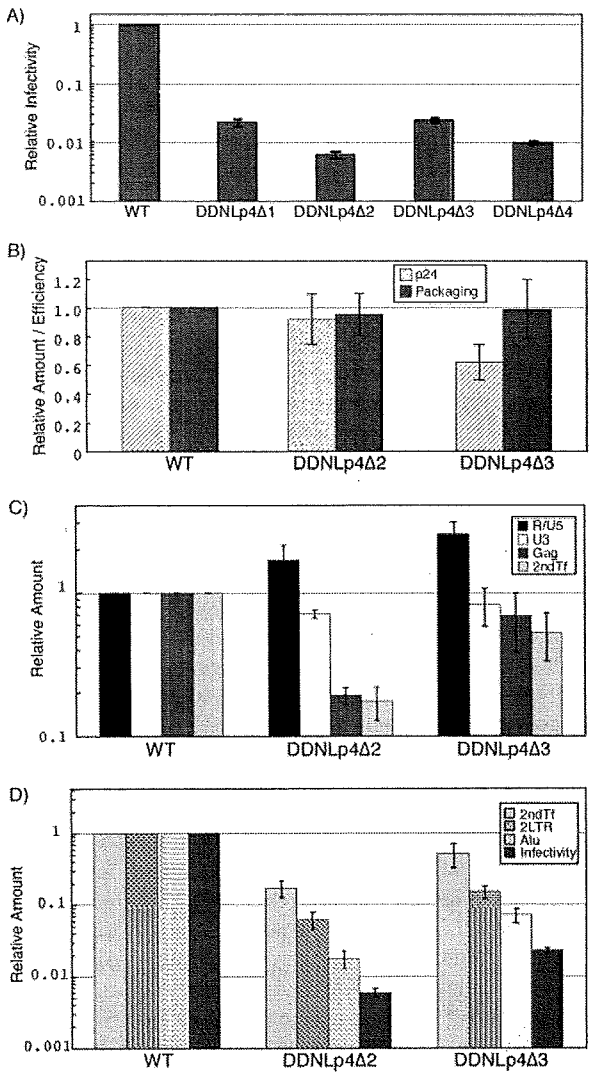

FIG. 4. Infectivity of mutant viruses. For each graph, the value of the WT was set at 1. Figures show the averages of results of at least two independent experiments. Error bars represent standard errors. (A) Single-round replication assay. M8166/H1Luc cells (1×10^6) were infected with the same quantity of CA-p24 of WT or mutant viruses pseudotyped with HIV-2 Env. At 24 to 48 h postinfection, cells were lysed and luciferase activity in the cell lysate was measured. (B) CA-p24 production and RNA packaging ability. Quantities of CA-p24 and viral RNA of purified virions were measured with the enzyme-linked immunosorbent assay and the RNase protection assay, respectively. Packaging efficiency was calculated by dividing the quantity of viral RNA by that of CA-p24. (C and D) Viral DNA quantification at early infection steps. A total of 1×10^6 MT-4 cells were infected with the same quantity of CA-p24 of WT or mutant viruses pseudotyped with HIV-2 Env. At 20 h postinfection, total cellular DNA was extracted and treated with DpnI overnight to digest methylated plasmid DNA. An equal amount of DNA was subjected to real-time PCR analysis. R/U5, strong-stop DNAs; U3, first-strand transferred products; Gag, negative-strand late products; 2ndTf, second-strand transferred products; 2LTR, 2-LTR viral circular DNA; Alu, PCR quantification for integrated proviral DNA; Infectivity, M8166/H1Luc cell assay as described for Fig. 4A.

Compared to the WT, a moderately large amount of DNA of both mutants was observed at the point of strong-stop DNA synthesis, which was reduced to a level similar to that of the WT in the subsequent first-strand transfer. At the next step, a big difference between the two mutants was observed. During the elongation of negative-strand DNA, the level of DNA synthesis of the DDNLp4Δ2 mutant was reduced to about 20%, whereas that of the DDNLp4Δ3 mutant remained at more than 60%. The level of DNA after the second-strand transfer showed additional moderate reduction for both of the mutants. As a result, a less than 50% reduction in overall viral cDNA production was observed in the DDNLp4Δ3 mutant, but a more than 80% reduction was observed in the DDNLp4Δ2 mutant. This result suggests that one of the defects was present at the reverse transcription stage. The reduction of the amounts of 2-LTR DNA, integrated DNA, and the infectivity are essentially similar between two mutants (Fig. 4D). As the 2-LTR circular DNA can be used as an indicator of RT completion and nuclear import of viral DNA (19), our findings suggest that the replication process from nuclear import to early gene expression was not specifically affected in a dimerization-defective mutant.

Attempt to generate replication-competent HIV-1 mutant containing monomeric genome. Multiround replication of a defective mutant virus sometimes results in the appearance of compensatory mutations to recover infectivity of the mutant without affecting viral RNA stability (38). Although we could not detect any efficient infectivity of mutant DDNLp4Δ2, we thought it might be possible to generate a replication-competent HIV-1 mutant containing a monomeric genome by means of long-term culture of infected cells. To verify this possibility, we constructed three mutants with Lp4Δ2 fragments on their genome, which retained all essential genes (*gag*, *pol*, *env*, *tat*, and *rev*) and important accessory genes (*vif* and *vpu*) but packaged the monomeric genome. Fragment Lp4Δ2 was inserted into *vpr*, *nef*, or both of pNL4-3 to construct pDDEE+, pDDXE+, and pDTEXE+, respectively (Fig. 5A). 293T cells were transfected with these constructs, the culture supernatants were harvested 2 to 3 days later, and the released virions collected. Roughly, the level of virion production by all three mutants was similar to that of the WT (data not shown). The genome from mutant virions contained 30 to 50% of monomeric genomes as shown by native Northern blotting analysis, thus confirming our previous observation (Fig. 5C). The mutants were examined for their ability to replicate in human $CD4^+$ cell lines MT-4 and M8166. Figure 6B shows the growth kinetics of the mutants in MT-4 cells. Mutant DTEXE+ was replication defective in MT-4 cells, while two mutants, DDEE+ and DDXE+, showed detectable virus replication but with growth kinetics that were significantly reduced and delayed compared to those of WT. On the other hand, all mutants were replication negative in M8166 cells (data not shown). Replicated viruses in the culture supernatant of MT-4 were harvested at their kinetic peak point. Equal amounts of RT units of virus samples were used for assay of reinfection of MT-4 cells, the remainder was centrifuged to purify virions, and the viral genome RNA was isolated. Growth kinetics of reinfected mutants restored their replication ability to a level comparable to that of the WT, suggesting that they had become revertants (data not shown). The results of native Northern blotting of genome RNA showed that MT-4 replicating mutants formed mostly dimers similar to that of the WT (Fig. 5D). Proviral genome sequencing from infected MT-4 chromosomal DNA proved that Lp4Δ2 sequences inserted in ectopic positions of the genome

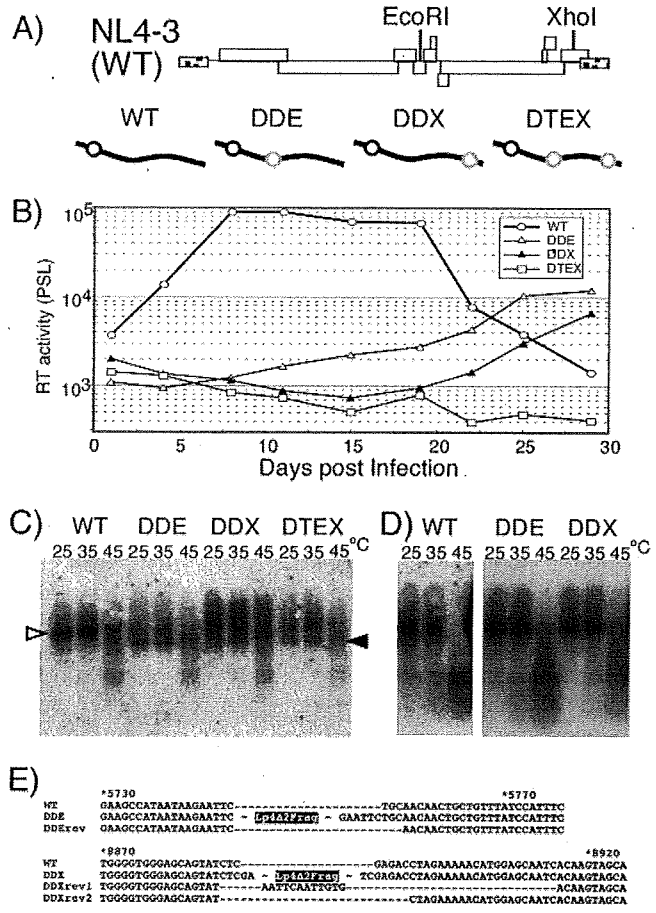

FIG. 5. Replication assay of mutants carrying a monomeric genome. (A) Schematic diagrams of replication-competent form mutants. The positions of restriction enzyme sites on the viral genome used for insertion are shown in the upper part of the panel. Diagrams of the mutants are shown in the lower part of the panel. Symbols are the same as those described for Fig. 3. (B) Growth kinetics of viruses. Values are representative of the results of at least three independent experiments. Viruses were prepared by transfection of 293T cells with pNL4-3 (WT) or its derivative mutants (pDDEE+ [DDE], pDDXE+ [DDX], and pDTEXE+ [DTE]). At 48 h posttransfection, culture supernatants of transfected 293T cells were harvested, and equal quantities of CA-p24 were inoculated into MT-4 cells. The supernatants of the cells were harvested every 3 or 4 days. Ten microliters of each cell supernatant was subjected to exogenous RT assay and quantitated by PhosphorImager analysis. PSL, Photostimulierte Lumineszenz. (C) Virion RNA profiles produced from transfected 293T cells and visualized by native Northern blotting analysis. Open and solid arrowheads denote positions of dimers and monomers, respectively. (D) Virion RNA profiles produced from MT-4 cells. Viruses were harvested at their growth kinetic peak point (wild type, 10 days postinfection; DDE and DDX, 28 days postinfection). (E) The nature of reversions. The sequences in the vicinity of the fragment-inserted sites are shown. The names of revertant sequences include "rev." The positions of Lp4Δ2 fragment insertion of DDE and DDX are indicated. The numbers above the sequences represent nucleotide positions of pNL4-3 (WT).

were completely deleted from both replication-competent mutants (Fig. 5E). Since the sequences of the revertants were found to contain an additional deletion or a small part of the inserted sequence at the mutated positions (Fig. 5E), the possibility of WT virus contamination could be ruled out.

DISCUSSION

The recent growth in interest in retrovirus genome dimerization has resulted in many publications that deal with its various aspects and that vary in depth and breadth (for reviews, see references 31, 35, and 37) Nonetheless, the overall picture of the retroviral dimerization signal remains unclear, so that there is still a need for detailed examination. The aim of the study reported here was to identify the minimal region sufficient for genome dimerization of HIV-1 in virions. In the first set of experiments, we defined the region sufficient for dimer linkage formation, and, in a subsequent experiment, we generated several deletion mutants to determine the minimal DLS required for HIV genome dimer linkage formation in virions. The minimal DLS identified in this study was only 144 bases long and included SL1, SL3, and SL4. Especially, SL1 deletion is more deleterious than is deletion of the other elements for dimer linkage formation in Fig. 2. It has been suggested that the hairpin loop of SL1 in DLS, known as DIS, plays a crucial role in dimerization and recombination (9, 33, 41). Our findings are well consistent with this notion.

While there are many functional regions for viral viability in the 5′ UTR of HIV, such as TAR, polyadenylation signal, PBS, and splicing donor, none was required for the dimerization function. This suggests that the genome dimerization of HIV-1 is independent of transactivation, splicing, or primer annealing. As we pointed out in a previous paper of ours (41) and in this study, the lower stem of the U5/L stem-loop is required for dimerization, which was not clearly identified during in vitro studies (for a review, see reference 30). This stem contains a so-called primer activation signal (5), which is thought to activate the initiation of reverse transcription. Since PBS or primer annealing is not required for dimerization, the involvement of primer activation signal and its opposing stem sequence in dimerization may be limited simply to creating a stable structure. Several studies have suggested that TAR, the R-U5 stem-loop region or coding region of *gag*, participates in the dimerization (4, 14, 16, 32) The contribution of those regions to RNA dimerization was demonstrated mainly in in vitro assays, but they were not included in the DLS identified in the in vivo assay used in our study. However, the possibility of a contribution by these regions cannot be ruled out since all mutants in our study retained the intact 5′ UTR. This result means that all mutants possess at least one set of the regions in the original position per genome, so that they may perform certain incidental functions for dimerization in virions.

Mfold RNA stability calculation (44) showed that the junction between R/U5 and U5/L stem-loops is relatively "free," which suggests that it is not involved in a base-pairing interaction with vicinal sequences (Fig. 1A). However, recent reports have suggested that the HIV-1 genome leader region could form an alternative structure known as the branched multiple hairpin (BMH) (1, 17). In this model, the 5′ junction sequence forms a stem structure with a sequence at the 3′ end of DLS. Although the BMH model was validated in an in vitro experiment, the DLS we defined in vivo was found to include all sequences required for the BMH formation. As an interaction between 5′ and 3′ ends of DLS should be essential for BMH formation, we evaluated the importance of both ends in vivo by making several base substitution mutants. The mutants con-

tained four to eight-base substitutions in either or both ends of the Lp4Δ2 fragment inserted in pDDNLp4Δ2. As expected, the 5′ or 3′ region of DLS appeared to be very important in dimer linkage formation of RNA since at least four-base substitutions (four substitutions in 8 bases of the 5′ end or four substitutions in 15 bases of the 3′ end) seriously disrupted the function (data not shown). Nonetheless, our attempt failed to yield a clear answer to whether BMH structure exists in virion RNA, probably because of difficulty in estimating the effect of the mutations on actual RNA shape in this region.

A noteworthy result of the M8166/H1Luc cell assay, an infectivity assay of monomeric genome mutants, was that the overall single-round infectivity of the mutant DDNLp4Δ2 was dramatically reduced (Fig. 4A). In our previous study, we reported that another monomeric genome mutant, DDNΔPBS, produced virions with less than 1% of infectivity of the WT (in one representative experiment, 1.4 versus 187.5 β-galactosidase-inducing units per ng of CA-p24 in a multinuclear activation of galactosidase indicator cell assay) (39). It well coincided with the data we got in the present study. As the inserted fragments of the four mutants were very similar in length and sequence (DDNLp4Δ1, 128 bases; DDNLp4Δ2, 144 bases; DDNLp4Δ3, 149 bases; and DDNLp4Δ4, 149 bases), a prominent replication defect of DDNLp4Δ2 might correlate with the appearance of monomeric genomes in virions, which is a unique feature of this mutant. Stepwise measurement of replication efficiency identified defects of the mutants in multiple steps of infection (Fig. 4C and D). Levels of viral DNA synthesis of DDNLp4Δ2 fell to around 15% of WT, whereas more than half of its viral DNA synthesis ability was retained in the DDNLp4Δ3 mutant. This difference strongly suggests a negative effect of the monomeric genome on reverse transcription. As the monomeric genome in virions of DDNLp4Δ2 accounted for 50% or less (Fig. 2B) of their content, the defect shown here occurred not only on the monomeric genome but also on the normal-looking dimeric genome of the mutants. These results seem to indicate that the inserted fragment of the mutant caused an abnormal secondary or tertiary structure of the overall viral RNA genome, resulting in poor reverse transcription. Viral genome dimerization and/or DIS was reported to play a role in efficient reverse transcription (6, 29), and our data supported these earlier arguments.

A multiround infection experiment clearly demonstrated significantly reduced growth kinetics of the mutants (Fig. 5). Moreover, inserted sequences of the mutants were completely deleted during the replication process, which strongly suggests that the insertion caused a fatal defect in viral replication. The appearance of revertants before the occurrence of compensation mutation implies that aberrant viral RNA conformation in these mutants was too drastic to be undone by protein modification.

In conclusion, in this study, we succeeded in identifying the essential region for HIV-1 genome dimer linkage formation in virions. Our consecutive experiments demonstrated that the dimerization region on RNA molecules may be important for the efficient progress of reverse transcription, probably by maintaining an appropriate form of viral genome in virions. A recent study has suggested that HIV-1 *pol* proteins contribute to genome RNA dimerization (8), which could be related to our speculation. Further studies can be expected to provide more findings relevant to this hypothesis.

ACKNOWLEDGMENTS

This work was supported by grants from the Ministry of Education, Culture, Sports, Science and Technology; the Ministry of Health, Labor, and Welfare; and the Health Science Foundation of Japan.

REFERENCES

1. **Abbink, T. E., and B. Berkhout.** 2003. A novel long distance base-pairing interaction in human immunodeficiency virus type 1 RNA occludes the Gag start codon. J. Biol. Chem. **278:**11601–11611.
2. **Adachi, A., H. E. Gendelman, S. Koenig, T. Folks, R. Willey, A. Rabson, and M. A. Martin.** 1986. Production of acquired immunodeficiency syndrome-associated retrovirus in human and nonhuman cells transfected with an infectious molecular clone. J. Virol. **59:**284–291.
3. **Aldovini, A., and B. D. Walker.** 1990. Techniques in HIV research. Stockton Press, New York, NY.
4. **Andersen, E. S., S. A. Contera, B. Knudsen, C. K. Damgaard, F. Besenbacher, and J. Kjems.** 2004. Role of the trans-activation response element in dimerization of HIV-1 RNA. J. Biol. Chem. **279:**22243–22249.
5. **Beerens, N., F. Groot, and B. Berkhout.** 2001. Initiation of HIV-1 reverse transcription is regulated by a primer activation signal. J. Biol. Chem. **276:** 31247–31256.
6. **Berkhout, B., A. T. Das, and J. L. van Wamel.** 1998. The native structure of the human immunodeficiency virus type 1 RNA genome is required for the first strand transfer of reverse transcription. Virology **249:**211–218.
7. **Brussel, A., and P. Sonigo.** 2003. Analysis of early human immunodeficiency virus type 1 DNA synthesis by use of a new sensitive assay for quantifying integrated provirus. J. Virol. **77:**10119–10124.
8. **Buxton, P., G. Tachedjian, and J. Mak.** 2005. Analysis of the contribution of reverse transcriptase and integrase proteins to retroviral RNA dimer conformation. J. Virol. **79:**6338–6348.
9. **Chin, M. P., T. D. Rhodes, J. Chen, W. Fu, and W. S. Hu.** 2005. Identification of a major restriction in HIV-1 intersubtype recombination. Proc. Natl. Acad. Sci. USA **102:**9002–9007.
10. **Darlix, J. L., C. Gabus, and B. Allain.** 1992. Analytical study of avian reticuloendotheliosis virus dimeric RNA generated in vivo and in vitro. J. Virol. **66:**7245–7252.
11. **Darlix, J. L., C. Gabus, M. T. Nugeyre, F. Clavel, and F. Barre-Sinoussi.** 1990. *cis* elements and *trans*-acting factors involved in the RNA dimerization of the human immunodeficiency virus HIV-1. J. Mol. Biol. **216:**689–699.
12. **Götte, M., X. Li, and M. A. Wainberg.** 1999. HIV-1 reverse transcription: a brief overview focused on structure-function relationships among molecules involved in initiation of the reaction. Arch. Biochem. Biophys. **365:**199–210.
13. **Graham, F. L., J. Smiley, W. C. Russell, and R. Nairn.** 1977. Characteristics of a human cell line transformed by DNA from human adenovirus type 5. J. Gen. Virol. **36:**59–74.
14. **Höglund, S., Å. Öhagen, J. Goncalves, A. T. Panganiban, and D. Gabuzda.** 1997. Ultrastructure of HIV-1 genomic RNA. Virology **233:**271–279.
15. **Hu, W. S., and H. M. Temin.** 1990. Retroviral recombination and reverse transcription. Science **250:**1227–1233.
16. **Huthoff, H., and B. Berkhout.** 2001. Mutations in the TAR hairpin affect the equilibrium between alternative conformations of the HIV-1 leader RNA. Nucleic Acids Res. **29:**2594–2600.
17. **Huthoff, H., and B. Berkhout.** 2001. Two alternating structures of the HIV-1 leader RNA. RNA **7:**143–157.
18. **Ikeda, T., H. Nishitsuji, X. Zhou, N. Nara, T. Ohashi, M. Kannagi, and T. Masuda.** 2004. Evaluation of the functional involvement of human immunodeficiency virus type 1 integrase in nuclear import of viral cDNA during acute infection. J. Virol. **78:**11563–11573.
19. **Julias, J. G., A. L. Ferris, P. L. Boyer, and S. H. Hughes.** 2001. Replication of phenotypically mixed human immunodeficiency virus type 1 virions containing catalytically active and catalytically inactive reverse transcriptase. J. Virol. **75:**6537–6546.
20. **Koh, K. B., M. Fujita, and A. Adachi.** 2000. Elimination of HIV-1 plasmid DNA from virus samples obtained from transfection by calcium-phosphate co-precipitation. J. Virol. Methods **90:**99–102.
21. **Marquet, R., F. Baudin, C. Gabus, J. L. Darlix, M. Mougel, C. Ehresmann, and B. Ehresmann.** 1991. Dimerization of human immunodeficiency virus (type 1) RNA: stimulation by cations and possible mechanism. Nucleic Acids Res. **19:**2349–2357.
22. **Marquet, R., J. C. Paillart, E. Skripkin, C. Ehresmann, and B. Ehresmann.** 1994. Dimerization of human immunodeficiency virus type 1 RNA involves sequences located upstream of the splice donor site. Nucleic Acids Res. **22:**145–151.
23. **McBride, M. S., and A. T. Panganiban.** 1996. The human immunodeficiency virus type 1 encapsidation site is a multipartite RNA element composed of functional hairpin structures. J. Virol. **70:**2963–2973.

24. **McBride, M. S., and A. T. Panganiban.** 1997. Position dependence of functional hairpins important for human immunodeficiency virus type 1 RNA encapsidation in vivo. J. Virol. **71**:2050–2058.
25. **McBride, M. S., M. D. Schwartz, and A. T. Panganiban.** 1997. Efficient encapsidation of human immunodeficiency virus type 1 vectors and further characterization of *cis* elements required for encapsidation. J. Virol. **71**: 4544–4554.
26. **Moumen, A., L. Polomack, B. Roques, H. Buc, and M. Negroni.** 2001. The HIV-1 repeated sequence R as a robust hot-spot for copy-choice recombination. Nucleic Acids Res. **29**:3814–3821.
27. **Nagao, T., A. Yoshida, A. Sakurai, A. Piroozmand, A. Jere, M. Fujita, T. Uchiyama, and A. Adachi.** 2004. Determination of HIV-1 infectivity by lymphocytic cell lines with integrated luciferase gene. Int. J. Mol. Med. **14**:1073–1076.
28. **Ohishi, M., T. Shioda, and J. I. Sakuragi.** 2007. Retro-transduction by virus pseudotyped with glycoprotein of vesicular stomatitis virus. Virology **362**: 131–138.
29. **Paillart, J. C., L. Berthoux, M. Ottmann, J. L. Darlix, R. Marquet, B. Ehresmann, and C. Ehresmann.** 1996. A dual role of the putative RNA dimerization initiation site of human immunodeficiency virus type 1 in genomic RNA packaging and proviral DNA synthesis. J. Virol. **70**:8348–8354.
30. **Paillart, J. C., R. Marquet, E. Skripkin, C. Ehresmann, and B. Ehresmann.** 1996. Dimerization of retroviral genomic RNAs: structural and functional implications. Biochimie **78**:639–653.
31. **Paillart, J. C., M. Shehu-Xhilaga, R. Marquet, and J. Mak.** 2004. Dimerization of retroviral RNA genomes: an inseparable pair. Nat. Rev. Microbiol. **2**:461–472.
32. **Paillart, J. C., E. Skripkin, B. Ehresmann, C. Ehresmann, and R. Marquet.** 2002. In vitro evidence for a long range pseudoknot in the 5′-untranslated and matrix coding regions of HIV-1 genomic RNA. J. Biol. Chem. **277**:5995–6004.
33. **Paillart, J. C., E. Skripkin, B. Ehresmann, C. Ehresmann, and R. Marquet.** 1996. A loop-loop "kissing" complex is the essential part of the dimer linkage of genomic HIV-1 RNA. Proc. Natl. Acad. Sci. USA **93**:5572–5577.
34. **Prats, A. C., C. Roy, P. A. Wang, M. Erard, V. Housset, C. Gabus, C. Paoletti, and J. L. Darlix.** 1990. *cis* elements and *trans*-acting factors involved in dimer formation of murine leukemia virus RNA. J. Virol. **64**:774–783.
35. **Rein, A.** 2004. Take two. Nat. Struct. Mol. Biol. **11**:1034–1035.
36. **Roy, C., N. Tounekti, M. Mougel, J. L. Darlix, C. Paoletti, C. Ehresmann, B. Ehresmann, and J. Paoletti.** 1990. An analytical study of the dimerization of in vitro generated RNA of Moloney murine leukemia virus MoMuLV. Nucleic Acids Res. **18**:7287–7292.
37. **Russell, R. S., C. Liang, and M. A. Wainberg.** 2004. Is HIV-1 RNA dimerization a prerequisite for packaging? Yes, no, probably? Retrovirology **1**:23.
38. **Russell, R. S., A. Roldan, M. Detorio, J. Hu, M. A. Wainberg, and C. Liang.** 2003. Effects of a single amino acid substitution within the p2 region of human immunodeficiency virus type 1 on packaging of spliced viral RNA. J. Virol. **77**:12986–12995.
39. **Sakuragi, J., A. Iwamoto, and T. Shioda.** 2002. Dissociation of genome dimerization from packaging functions and virion maturation of human immunodeficiency virus type 1. J. Virol. **76**:959–967.
40. **Sakuragi, J., T. Shioda, and A. T. Panganiban.** 2001. Duplication of the primary encapsidation and dimer linkage region of HIV-1 RNA results in the appearance of monomeric RNA in virions. J. Virol. **75**:2557–2565.
41. **Sakuragi, J., S. Ueda, A. Iwamoto, and T. Shioda.** 2003. Possible role of dimerization in human immunodeficiency virus type 1 genome RNA packaging. J. Virol. **77**:4060–4069.
42. **Sakuragi, J. I., and A. T. Panganiban.** 1997. Human immunodeficiency virus type 1 RNA outside the primary encapsidation and dimer linkage region affects RNA dimer stability in vivo. J. Virol. **71**:3250–3254.
43. **Willey, R. L., D. H. Smith, L. A. Lasky, T. S. Theodore, P. L. Earl, B. Moss, D. J. Capon, and M. A. Martin.** 1988. In vitro mutagenesis identifies a region within the envelope gene of the human immunodeficiency virus that is critical for infectivity. J. Virol. **62**:139–147.
44. **Zuker, M.** 1989. On finding all suboptimal foldings of an RNA molecule. Science **244**:48–52.

THE JOURNAL OF BIOLOGICAL CHEMISTRY VOL. 282, NO. 39, pp. 28709–28720, September 28, 2007
Printed in the U.S.A.

Potent Inhibition of HIV-1 Replication by Novel Non-peptidyl Small Molecule Inhibitors of Protease Dimerization*

Received for publication, May 14, 2007, and in revised form, June 25, 2007 Published, JBC Papers in Press, July 17, 2007, DOI 10.1074/jbc.M703938200

Yasuhiro Koh[‡§], Shintaro Matsumi[‡§], Debananda Das[¶], Masayuki Amano[‡§], David A. Davis[‖], Jianfeng Li[**], Sofiya Leschenko[**], Abigail Baldridge[**], Tatsuo Shioda[‡‡], Robert Yarchoan[‖], Arun K. Ghosh[**], and Hiroaki Mitsuya[‡§¶1]

From the [‡]Department of Hematology and [§]Department of Infectious Diseases, Kumamoto University Graduate School of Medical and Pharmaceutical Sciences, 1-1-1 Honjo, Kumamoto 860-8556, Japan, the [¶]Experimental Retrovirology Section and [‖]Retroviral Disease Section, HIV and AIDS Malignancy Branch, NCI, National Institutes of Health, Bethesda, Maryland 20892, the [**]Departments of Chemistry and Medicinal Chemistry, Purdue University, West Lafayette, Indiana 47907, and the [‡‡]Department of Viral Infections, Research Institute for Microbial Diseases, Osaka University, Osaka 565-0871, Japan

Dimerization of HIV-1 protease subunits is essential for its proteolytic activity, which plays a critical role in HIV-1 replication. Hence, the inhibition of protease dimerization represents a unique target for potential intervention of HIV-1. We developed an intermolecular fluorescence resonance energy transfer-based HIV-1-expression assay employing cyan and yellow fluorescent protein-tagged protease monomers. Using this assay, we identified non-peptidyl small molecule inhibitors of protease dimerization. These inhibitors, including darunavir and two experimental protease inhibitors, blocked protease dimerization at concentrations of as low as 0.01 μM and blocked HIV-1 replication with IC_{50} values of 0.0002–0.48 μM. These agents also inhibited the proteolytic activity of mature protease. Other approved anti-HIV-1 agents examined except tipranavir, a CCR5 inhibitor, and soluble CD4 failed to block the dimerization event. Once protease monomers dimerize to become mature protease, mature protease is not dissociated by this dimerization inhibition mechanism, suggesting that these agents block dimerization at the nascent stage of protease maturation. The proteolytic activity of mature protease that managed to undergo dimerization despite the presence of these agents is likely to be inhibited by the same agents acting as conventional protease inhibitors. Such a dual inhibition mechanism should lead to highly potent inhibition of HIV-1.

Highly active antiretroviral therapy has had a major impact on the AIDS epidemic in industrially advanced nations. However, eradication of human immunodeficiency virus, type 1 (HIV-1)[2] does not appear to be currently possible, in part due to the viral reservoirs remaining in blood and infected tissues. Moreover, a number of challenges have been encountered, which include various adverse effects, only partial and limited immunologic restorations achieved, and occurrence of various cancers as consequences of survival elongation with highly active antiretroviral therapy (1). Moreover, such limitations of highly active antiretroviral therapy are exacerbated by the development of drug-resistant HIV-1 variants (2). Thus, the identification of new classes of antiretroviral drugs that have one or more unique mechanisms of action and produce no or minimal adverse effects remains an important therapeutic objective.

Dimerization of HIV-1 protease subunits is an essential process for the acquisition of proteolytic activity of HIV-1 protease, which plays a critical role in the maturation and replication of the virus (3, 4). Thus inhibition of protease dimerization by chemical reagents is likely to abolish proteolytic activity and inhibit HIV-1 replication. However, for possible development of HIV-1 protease dimerization inhibitors, better understanding of the nature and dynamics of protease dimerization is crucial. The monomer subunits are connected by polar and non-polar interactions to form the dimer. Hydrophobicity of Leu-89, Leu-90, and Ile-93 and several other residues have been considered important in the folding of a protease monomer as well as in dimer stabilization (5, 6). For a systematic analysis of the conserved network of hydrogen bonds, termed "fireman's grip," Strisovsky *et al.* (7) have mutated the active site Thr-26 to a Ser, Cys, or Ala and have shown that T26A substitution reduced protease dimer stability, thus virtually nullifying the proteolytic activity of protease. Indeed, in our present study, T26A substitution effectively disrupted protease dimerization (see below), corroborating the results by Strisovsky *et al.* The flexibility of monomeric and dimeric HIV-1 protease and the feasibility of a stable protease monomer have also been studied

* This work was supported by the Intramural Research Program of Center for Cancer Research, NCI, National Institutes of Health (NIH), by a Grant-in-aid for Scientific Research (Priority Areas) from the Ministry of Education, Culture, Sports, Science, and Technology of Japan (Monbu-Kagakusho), a Grant for Promotion of AIDS Research from the Ministry of Health, Welfare, and Labor of Japan (Kosei-Rohdosho), by the Cooperative Research Project on Clinical and Epidemiological Studies of Emerging and Re-emerging Infectious Diseases (Renkei Jigyo: Grant 78, Kumamoto University) of Monbu-Kagakusho, by the Japan Health Sciences Foundation (International Research Grant SA14801 to H. M. and A. K. G.), and by NIH Grant GM 53386 (to A. K. G.). The costs of publication of this article were defrayed in part by the payment of page charges. This article must therefore be hereby marked "*advertisement*" in accordance with 18 U.S.C. Section 1734 solely to indicate this fact.

[1] To whom correspondence should be addressed: Tel.: 81-96-373-5156; Fax: 81-96-363-5265; E-mail: hmitsuya@helix.nih.gov.

[2] The abbreviations used are: HIV-1, human immunodeficiency virus, type 1; FRET, fluorescence resonance energy transfer; CFP, cyan fluorescent protein; YFP, yellow fluorescent protein; BCV, brecanavir; DRV, darunavir; CHX, cycloheximide; PI, protease inhibitor; bis-THF, bistetrahydrofuranylurethane; TPV, tipranavir; Fluc, firefly luminescence; Rluc, *Renilla* luminescence; RT, reverse transcriptase; PR, protease.

by computational simulation (8, 9). There are four anti-parallel β-sheets involving the N and C termini of both monomer subunits and they contribute close to 75% of the dimerization energy (10), explaining at least in part why DRV failed to dissociate mature protease dimer (see below). The termini interface has been explored as a dimerization inhibition target by several groups (11–13). We have also recently reported that certain peptides containing the dimer interface sequences amino acids 1–5 and amino acids 95–99 blocked HIV-1 infectivity and replication (14). However, to the best of our knowledge, no evidence of direct dimerization inhibition by such compounds has been yet documented.

In the present study, we developed an intermolecular fluorescence resonance energy transfer (FRET)-based HIV-1-expression assay that employed cyan and yellow fluorescent protein-tagged HIV-1 protease monomers. Using this assay, we identified a group of non-peptidyl small molecule inhibitors of HIV-1 protease dimerization. These inhibitors, including the recently approved protease inhibitor (PI) darunavir (DRV) as well as two experimental protease inhibitors (PIs), blocked protease dimerization at concentrations of as low as 0.01 μM and blocked HIV-1 replication *in vitro* with IC_{50} values of 0.0002–0.48 μM. These agents also inhibited the proteolytic activity of mature HIV-1 protease. Another PI, tipranavir (TPV), active against HIV-1 variants resistant to multiple PIs, also blocked protease dimerization, although all other existing FDA-approved anti-HIV-1 drugs examined in the present study failed to block the dimerization. The present report represents the first demonstration that non-peptidic small molecule agents can disrupt protease dimerization.

EXPERIMENTAL PROCEDURES

Generation of FRET-based HIV-1 Expression System—Cyan fluorescent protein (CFP)- and yellow fluorescent protein (YFP)-tagged HIV-1 protease constructs were generated using BD Creator™ DNA cloning kits (BD Biosciences, San Jose, CA). First, XhoI/HindIII fragments from pCR-XL-TOPO vector containing the HIV-1 protease-encoding gene excised from pHIV-1_{NL4-3} was inserted into the pDNR-1r (donor vector) that had been digested with XhoI and HindIII. In the transfer of the protease gene from the donor vector into pLP-CFP/YFP-C1 (acceptor vector), the Cre-loxP site-specific recombination method was used according to manufacturer's instructions. Using Cre-recombinase with the lox P site, the protease gene from pDNR-1r was inserted into pLP-CFP-C1 or pLP-YFP-C1 through Cre-mediated recombination (15), generating a plasmid of CFP-tagged wild type protease (PR_{WT}) and that of YFP-tagged PR_{WT}, with which HIV-1 protease was successfully expressed as a fusion protein with CFP- and YFP-tagged at the C terminus, respectively. Western blot assay using anti-green fluorescent protein-specific rabbit polyclonal antibodies revealed that protease was correctly tagged to CFP or YFP (data not shown).

For the generation of full-length molecular infectious clones containing CFP- or YFP-tagged protease, the PCR-mediated recombination method was used (16). To this end, we amplified an upstream proviral DNA fragment containing ApaI site and HIV-1 protease (excised from pHIV-1_{NL4-3}) with a primer pair: Apa-PRO-F (5′-TTG CAG GGC CCC TAG GAA AAA GG-3′) plus PR-5Ala-R (5′-GGC TGC TGC GGC AGC AAA ATT TAA AGT GCA GCC AAT CT-3′), a middle proviral DNA fragment containing CFP (excised from pCFP-C1) or YFP (excised from pYFP-C1) (Clontech, Mountain View, CA) with a primer pair: CFPYFP-5Ala-F (5′-GCT GCC GCA GCA GCC GTG AGC AAG GGC GAG GAG CTG-3′) plus CFPYFP-FP-R (5′-ACT AAT GGG AAA CTT GTA CAG CTC GTC CAT GCC G-3′), and a downstream proviral DNA fragment containing the 5′-DNA fragment of reverse transcriptase (RT) and SmaI site from pHIV-1_{NLSma} (17), which had been created to have a SmaI site by changing two nucleotides (2590 and 2593) of pHIV-1_{NL4-3} with a primer pair: FRT-F (5′-TTT CCC ATT AGT CCT ATT GAG ACT GTA-3′) plus NL4-3-RT263-R (5′-CCA GAA ATC TTG AGT TCT CTT ATT-3′). A linker consisting of five alanines was inserted between protease and fluorescent protein. The phenylalanine-proline site that HIV-1 protease cleaves was also introduced between the fluorescent protein and RT. Thus obtained three DNA fragments were subsequently joined by using the PMR reaction performed under the standard condition for ExTaq polymerase (Takara Bio Inc., Otsu, Japan) with 10 pmol of Apa-PRO-F (5′-TTG CAG GGC CCC TAG GAA AAA GG-3′) and NL4-3-RT263-R (5′-CCA GAA ATC TTG AGT TCT CTT ATT-3′) and the three DNA fragments (100 ng each) in a 20-μl reaction solution. Thermal cycling was carried out as follows: 94 °C for 3 min, followed by 35 cycles of 94 °C for 50 s, 53 °C for 50 s, and 72 °C for 2 min, and finally by 72 °C for 15 min. The amplified PCR products were cloned into pCR-XL-TOPO vector according to the manufacturer's instructions (Gateway Cloning System, Invitrogen). PCR products were generated with pCR-XL-TOPO vector as templates, followed by digestion by both ApaI and SmaI, and the ApaI-SmaI fragment was introduced into pHIV-1_{NLSma} (17), generating pHIV-PR_{WT}^{CFP} and pHIV-PR_{WT}^{YFP}, respectively.

Analysis of Inter- and Intra-molecule Interactions of Protease Subunits—Analysis of inter- and intra-molecule interactions of protease subunits was conducted by employing the crystal structure of DRV with HIV-1 protease (PDB ID: 2IEN). Hydrogens were added and minimized using the OPLS2005 force field with constraints on heavy atom positions. The calculation was performed using MacroModel 9.1 from Schrödinger, LLC. Hydrogen bonds were assigned when the following distance and angle cut-off was satisfied: 3.0 Å for H-A distance; D-H-A angle >90°; and H-A-B angle >60° where H is the hydrogen, A is the acceptor, D is the donor, and B is a neighbor atom bonded to the acceptor. The representative distance between the termini of two monomers was determined by analyzing the protease-DRV crystal structure (PDB ID: 2IEN). The distance between the α carbons at the N termini and C termini is around 0.5 nm, whereas the distance between the α carbons of the N termini ends of two monomers is around 1.8 nm.

FRET Procedure—COS7 cells plated on EZ view cover-glass bottom culture plate (Iwaki, Tokyo) were transfected with the indicated plasmid constructs using Lipofectamine 2000 (Invitrogen) according to manufacturer's instructions in the presence of various concentrations of each compound, cultured for 72 h, and analyzed under Fluoview FV500 confocal laser scanning microscope (Olympus Optical Corp., Tokyo) at room

temperature. When the effect of each compound was analyzed by FRET, test compounds were added to the culture medium simultaneously with plasmid transfection.

The results of FRET were determined by quenching of CFP (donor) fluorescence and an increase in YFP (acceptor) fluorescence (sensitized emission), because part of the energy of CFP is transferred to YFP instead of being emitted. This phenomenon can be measured by bleaching YFP, which should result in an increase in CFP fluorescence. This technique, also known as acceptor photobleaching, is a well established method of determining the occurrence of FRET (18–21). Dequenching of the donor CFP by selective photobleaching of the acceptor YFP was performed by first obtaining YFP and CFP images at the same focal plane, followed by illuminating for 3 min the same image at a wavelength of 488 nm with a laser power set at the maximum intensity to bleach YFP and re-capturing the same CFP and YFP images. The changes in the CFP and YFP fluorescence intensity in the images of selected regions were examined and quantified using Olympus FV500 Image software system (Olympus Optical Corp.). Background values were obtained from the regions where no cells were present and were subtracted from the values for the cells examined in all calculations. For each chimeric protein, the data were obtained from at least three independent experiments. Digitized image data obtained from the experiment were prepared for presentation using Photoshop 6.0 (Adobe Systems, Mountain View, CA). Ratios of intensities of CFP fluorescence after photobleaching to CFP fluorescence prior to photobleaching ($CFP^{A/B}$ ratios) were determined. It is well established that the $CFP^{A/B}$ ratios of >1.0 indicate that association of CFP- and YFP-tagged proteins occurred, and it was interpreted that the dimerization of protease subunits occurred. When the $CFP^{A/B}$ ratios were <1, it indicated that the association of the two subunits did not occur, and it was interpreted that protease dimerization was inhibited.

Non-peptidyl Small Molecule Compounds—Seven non-peptidyl small molecule compounds were synthesized in a convergent manner by coupling an optically active P2 ligand and an (*R*)-hydroxyethylamino sulfonamide isostere (22). Synthetic methods for TMC126 and DRV have been previously described (22, 23). Detailed synthetic methods for the other four compounds will be described elsewhere. TPV was obtained through the AIDS Research and Reference Reagent Program, Division of AIDS, NIAID, National Institutes of Health.

Dual Luciferase Assay—Dual luciferase assay was established using the CheckMate™ Mammalian Two-Hybrid System (Promega Corp., Madison, WI). Briefly, BamHI/KpnI fragments from pCR-XL-TOPO vector containing the HIV-1 protease (PR_{WT})-encoding gene excised from pHIV-1_{NL4-3} was inserted into the pACT vector and pBIND vector that had been digested with BamHI and KpnI, generating pACT-PR_{wt} and pBIND-PR_{wt}, which produced an in-frame fusion of wild-type HIV-1 protease downstream of the VP16 activation domain and GAL4 DNA-binding domain, respectively. COS7 cells were co-transfected with pACT-PR_{wt}, pBIND-PR_{wt}, and pG5*luc* in the absence or presence of 0.1 or 1.0 μM DRV in white 96-well flat bottom plates (Corning, NY), cultured for 48 h, and the intensity of firefly luminescence (Fluc) and *Renilla* luminescence (Rluc) was measured with TR717 microplate luminometer (Applied Biosystems) according to the manufacturer's instructions. DRV was added to the culture medium simultaneously with plasmids to be used. Fluc/Rluc intensity ratios were determined with co-transfection of pACT-PR_{WT}, pBIND-PR_{WT}, and pG5*luc* in the absence of DRV, serving as maximal values. Fluc/Rluc intensity ratios determined with co-transfection of a pACT vector, a pBIND vector, and pG5*luc* served as minimal (background) values. Relative response ratios (RRR) were determined using the following formula: RRR = [(experimental Fluc/Rluc) − (negative control Fluc/Rluc)]/[(positive control Fluc/Rluc) − (negative control Fluc/Rluc)].

Drug Susceptibility Assay—The susceptibility of HIV-1_{LAI} to various drugs and their cytotoxicity were determined using the 3-(4,5-dimethylthiazol-2-yl)-2,5-diphenyltetrazolium bromide assay as previously described (24). Briefly, MT-2 cells (2×10^4/ml) were exposed to 100 50% tissue culture infectious doses ($TCID_{50}$s) of HIV-1_{LAI} in the presence or absence of various concentrations of drugs in 96-well microculture plates and cultured at 37 °C for 7 days. After 100 μl of the medium was removed from each well, 3-(4,5-dimetylthiazol-2-yl)-2,5-diphenyltetrazolium bromide solution (10 μl, 7.5 mg/ml in phosphate-buffered saline) was added to each well, followed by incubation at 37 °C for 4 h. After incubation, 100 μl of acidified isopropanol containing 4% (v/v) Triton X-100 was added to each well, to dissolve the formazan crystals, and the optical density was measured in a kinetic microplate reader (V_{max}, Molecular Devices, Sunnyvale, CA). All assays were performed in duplicate or triplicate. In some experiments, MT-2 cells were chosen as target cells in the 3-(4,5-dimethylthiazol-2-yl)-2,5-diphenyltetrazolium bromide assay, because these cells undergo greater HIV-1-elicited cytopathic effects than MT-4 cells.

Enzyme Kinetics—The chromogenic substrate Lys-Ala-Arg-Val-Nle-paranitro-Phe-Glu-Ala-Nle-amide (Sigma) was used to determine the kinetic parameters (25, 26). Wild-type protease, at final concentrations of 160–190 nM, was added to varying concentrations of substrate (100–400 μM) maintained in 50 mM sodium acetate (pH 5.0), 0.1 M NaCl, 1 mM EDTA, and assayed by monitoring the decrease in absorbance at 310 nm using a Varian Cary 100Bio UV-visible spectrophotometer. The k_{cat} and K_m values were obtained employing standard data fitting techniques for a reaction obeying Michaelis-Menten kinetics. The data curves were fitted using SigmaPlot 8.0.2 (SPSS Inc., Chicago, IL). The active enzyme concentrations were calculated from the intercept of the linear fit to the IC_{50} *versus* [S] plots with the IC_{50} axis. The K_i values were obtained from the IC_{50} values estimated from an inhibitor dose-response curve with the spectroscopic assay using the equation $K_i = (IC_{50} - [E]/2)/(1 + [S]/K_m)$, where [*E*] and [S] are the protease and substrate concentrations, respectively (27). The K_i values were measured at four to five substrate concentrations. The measurement was repeated at least three times to produce the average values.

Assay for Effects of Darunavir on Dimerized Mature Protease—To examine whether a representative dimerization inhibitor, DRV, could dissociate mature protease that had already been

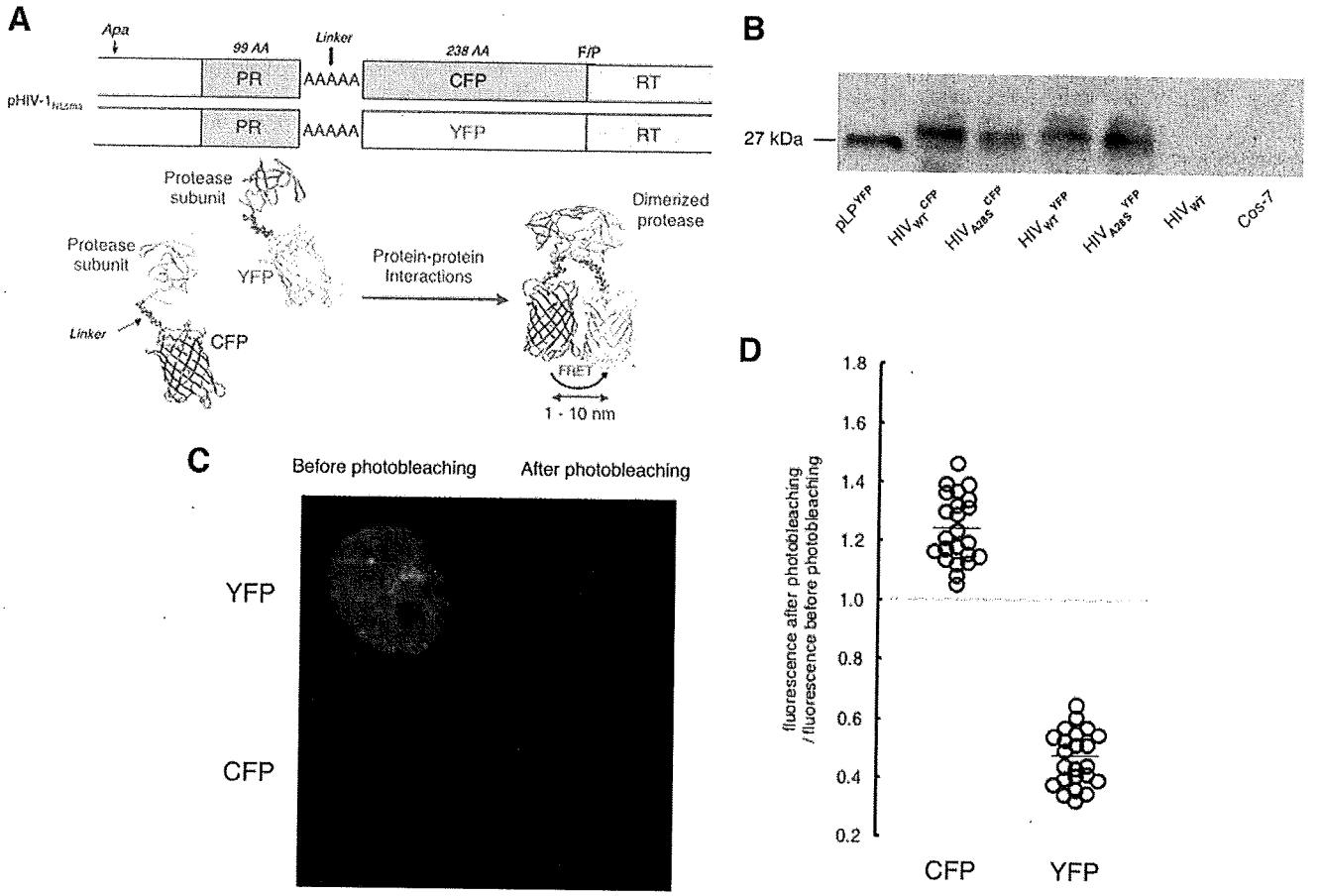

FIGURE 1. **FRET-based HIV-1 expression system.** *A*, generation of FRET-based HIV-1 expression system. Various plasmids encoding full-length molecular infectious HIV-1 (HIV-1_{NL4-3}) clones producing CFP- or YFP-tagged protease using the PCR-mediated recombination method were prepared. A linker consisting of five alanines was inserted between protease and fluorescent protein. A phenylalanine-proline site (*F/P*) that HIV-1 protease cleaves was also introduced between the fluorescent protein and RT. Shown are structural representations of protease monomers and dimer in association with the linker atoms and fluorescent proteins. FRET occurs only when the fluorescent proteins are 1–10 nm apart. *B*, expression of CFP- and YFP-tagged wild-type HIV-1 protease. To confirm the presence of HIV-1 protease tagged to fluorescent protein in COS7 cells transfected with a plasmid encoding $HIV_{WT}{}^{CFP}$, $HIV_{A28S}{}^{CFP}$, $HIV_{WT}{}^{YFP}$, or $HIV_{A28S}{}^{YFP}$, Western blot analysis was performed using lysates of pelleted virions. The CFP- and YFP-tagged proteases were visualized by SuperSignal WestPico Chemiluminescent Substrates using polyclonal anti-GFP antiserum and ECL anti-rabbit IgG peroxidase-linked species-specific whole antibody. pLP^{YFP} denotes the lysates of cells transfected with a plasmid encoding only YFP. The lysates of COS7 cells transfected with a plasmid encoding HIV_{WT}, and those of untreated COS7 cells serve as controls. *C*, fluorescence images of co-transfected cells prior to and after acceptor photobleaching. COS7 cells plated on EZ view cover-glass bottom culture plate were transfected with two plasmids, $pPR_{WT}{}^{CFP}$ and $pPR_{WT}{}^{YFP}$, using Lipofectamine, cultured for 72 h, and analyzed under a Fluoview FV500 confocal laser scanning microscope. Both $PR_{WT}{}^{CFP}$ and $PR_{WT}{}^{YFP}$ proteins were visualized prior to photobleaching. Note that photobleaching of the cells dramatically reduced YFP fluorescence with a $YFP^{A/B}$ ratio of 0.17 and increased CFP emission with a $CFP^{A/B}$ ratio of 1.38, signifying the dimerization of both YFP- and CFP-tagged protease subunits. *D*, ratios of the emission intensities before and after photobleaching. Fluorescence intensities of each cell transfected with two plasmids, $pPR_{WT}{}^{CFP}$ and $pPR_{WT}{}^{YFP}$, were measured before and after photobleaching, and ratios of the emission intensities before and after photobleaching ($CFP^{A/B}$ ratios) were determined, and plotted. The $CFP^{A/B}$ ratio values were 1.24 ± 0.11 (n = 23), whereas the $YFP^{A/B}$ ratio values were 0.47 ± 0.09 (n = 23). The mean of these ratios are shown as *bars*.

dimerized, COS7 cells were co-transfected with a pair of plasmids encoding HIV-$PR_{WT}{}^{CFP}$ and HIV-$PR_{WT}{}^{YFP}$ and exposed to a protein synthesis inhibitor cycloheximide (CHX, 50 μg/ml, Sigma) at 24, 48, 72, and 96 h of culture following transfection. The cells were then exposed to DRV (1 μM) on day 5 of culture, and the values of the $CFP^{A/B}$ ratio were determined at various time points. When the $CFP^{A/B}$ ratios determined were >1.0, it was determined that HIV-1 protease had been generated and dimerization had occurred. The production of HIV-1 was monitored every 24 h following transfection by determining levels of p24 Gag protein produced into culture medium as previously described (24).

RESULTS

Generation of FRET-based HIV-1 Expression Assay—The basic concepts of the intermolecular FRET-based HIV-1-expression assay (FRET-HIV-1 assay) are shown in Fig. 1. Within a plasmid (pHIV-1_{NL4-3}), which encodes a full-length molecular infectious HIV-1 clone, the gene encoding a CFP was attached to the downstream end (C terminus) of the gene encoding an HIV-1 protease subunit through the flexible linker added (five alanines), generating pHIV-$1_{NL4-3/CFP}$ (Fig. 1*A*). Within the other plasmid (pHIV-1_{NL4-3}), the gene encoding a YFP was attached to the downstream end of protease-encoding gene in the same manner, generating pHIV-$1_{NL4-3/YFP}$. Both CFP and YFP were designed to have phenylalanine and proline in the connection with RT so that the protease is cleaved from RT when two subunits dimerize and the dimerized protease acquires enzymatic activity. Fig. 1*B* illustrates that HIV-1 virions generated in COS7 cells transfected with pHIV-$1_{NL4-3/CFP}$ contained CFP-tagged protease and those in COS7 cells transfected with pHIV-$1_{NL4-3/YFP}$ contained YFP-tagged protease as

examined in Western blotting. The HIV-1 virions produced were capable of infecting $CD4^+$ MT-4 cells when the cells were exposed to the supernatant of the transfected COS7 cells (data not shown), indicating that the expressed tagged protease was enzymatically and virologically functional. In the cytoplasm of COS7 cells co-transfected with pHIV-$1_{NL4\text{-}3/CFP}$ and pHIV-$1_{NL4\text{-}3/YFP}$, a CFP-tagged protease subunit interacts and dimerizes with a YFP-tagged protease subunit, and CFP and YFP get close because the termini are separated by only 0.5 to 1.8 nm in the dimeric form of protease (note: the representative distance was determined by analyzing the protease-DRV crystal structure (PDB ID: 2IEN)). A focused laser beam excitation of CFP (triggered by helium-cadmium laser) results in rapid energy transfer to YFP, and most of the fluorescence photons are emitted by YFP (28). If the dimerization is blocked, the average distance between CFP and YFP become larger, the energy transfer rate is decreased, and the fraction of photons emitted by YFP is lowered.

To help us interpret the energy transfer efficiency quantitatively, we used the acceptor photobleaching technique, in which the change in CFP emission quenching is measured by comparing the value before and after selectively photobleaching YFP, which prevents problems associated with variable expression levels. In this acceptor photobleaching approach, when FRET occurs, the fluorescence of the CFP donor increases after bleaching the YFP acceptor chromophore, which is recognized as a signature for FRET (18). Thus, the analysis of the change in CFP fluorescence intensity in the same specimen regions, before and after removal of the acceptor, directly relates the energy transfer efficiency to both donor and acceptor fluorescence. Fig. 1*C* illustrates representative images of co-transfected cells prior to and after YFP photobleaching, showing that, following photobleaching, YFP fluorescence of YFP-tagged wild-type protease subunit ($PR_{WT}{}^{YFP}$) was decreased, whereas CFP fluorescence of $PR_{WT}{}^{CFP}$ increased.

To further help us evaluate the energy transfer efficiency, we determined the ratios of cyan fluorescence intensity, determined with a confocal laser scanning microscope, after photobleaching over that before photobleaching (hereafter referred to as $CFP^{A/B}$ ratios). We also determined $YFP^{A/B}$ ratios in the same manner. If the $CFP^{A/B}$ ratios are >1.0, it is thought the energy transfer (or FRET) took place (18), signifying that dimerization of $PR_{WT}{}^{CFP}$ and $PR_{WT}{}^{YFP}$ subunits occurred. Fig. 1*D* shows that in the co-transfected COS7 cells (n = 23), the $CFP^{A/B}$ ratios were all >1.0 ($CFP^{A/B}$ ratios, 1.24 ± 0.11; $YFP^{A/B}$ ratios, 0.47 ± 0.09), demonstrating that dimerization of protease subunits occurred.

Changes in Fluorescence Emission with Amino Acid Substitutions in Protease—First, it was determined whether the above-described FRET-HIV-1 assay could be used to detect the disruption of HIV-1 protease dimerization. Five amino acids at the N terminus and those at the C terminus have been shown to be critical for protease dimerization (29). As shown in Fig. 2*A*, two protease monomer subunits are connected by four antiparallel β-sheets involving the N and C termini of both subunits. It is of note that mature dimerized protease has as many as 12 hydrogen bonds in this N- and C-terminal region. Thus, we introduced a Pro-1 to Ala substitution (P1A), Q2A, I3A, T4A, L5A, T96A, L97A, N98A, or F99A substitution into the replication-competent HIV-$1_{NL4\text{-}3}$ and found that I3A, L5A, T96A, L97A, and F99A disrupted protease dimerization, although other substitutions did not disrupt the dimerization.

Several amino acid substitutions outside the N and C termini have also been known to play a role in HIV-1 protease dimerization. Ishima and Louis and their colleagues have demonstrated that the introduction of T26A, D29N, D29A, or R87K to HIV-1 protease disrupts the dimer interface contacts and destabilizes protease dimer, causing the inhibition of protease dimerization (30–32). Fig. 2 (*B* and *C*) shows the locations of intermolecular hydrogen bonds formed by such amino acids between two monomer subunits. The hydrogen bond interactions between two subunits occur between Asp-29 and Arg-8′, Arg-87 and Leu-5′, Leu-24 and Thr-26′, and Thr-26 and Thr-26′. There are also intra-molecular hydrogen bond interactions between Asp-29 and Arg-87 as shown in Fig. 2 (*B–D*). Thus, mutations in those amino acids were introduced into HIV-$PR_{WT}{}^{CFP}$ and HIV-$PR_{WT}{}^{YFP}$, generating HIV-$PR_{T26A}{}^{CFP}$, HIV-$PR_{T26A}{}^{YFP}$, HIV-$PR_{D29N}{}^{CFP}$, HIV-$PR_{D29N}{}^{YFP}$, HIV-$PR_{D29A}{}^{CFP}$, HIV-$PR_{D29A}{}^{YFP}$, HIV-$PR_{R87K}{}^{CFP}$, and HIV-$PR_{R87K}{}^{YFP}$. Co-transfection of COS7 cells with a pair of CFP- and YFP-tagged protease-carrying HIV-1-encoding plasmids demonstrated that these four amino acid substitutions disrupted protease dimerization (the average $CFP^{A/B}$ ratios were all <1.0; Fig. 2*E*). Substitutions of two amino acids adjacent to Asp-29 were also introduced, generating HIV-$PR_{A28S}{}^{CFP}$, HIV-$PR_{A28S}{}^{YFP}$, HIV-$PR_{D30N}{}^{CFP}$, and HIV-$PR_{D30N}{}^{YFP}$. Both A28S and D30N are known primary amino acid substitutions, conferring resistance to TMC126 and nelfinavir on HIV-1, respectively (33, 34). The fact that A28S- or D30N-containing HIV-1 is infectious and replication-competent indicates that these two amino acid substitutions would not disrupt protease dimerization. HIV-1 virions generated in COS7 cells transfected with HIV-$PR_{A28S}{}^{CFP}$ and HIV-$PR_{A28S}{}^{YFP}$ were confirmed to contain CFP-tagged protease and YFP-tagged protease in Western blotting, respectively (Fig. 1*B*). As expected, neither substitution disrupted the dimerization as examined in the FRET-HIV-1 assay (Fig. 2*E*). Another mutation D25A, which is adjacent to Thr^{26} and is known to abrogate replicative activity of HIV-1 (35), failed to disrupt protease dimerization, indicating that the inability of D25A mutation-carrying HIV-1 to replicate is not due to dimerization disruption, but due to the loss of proteolytic activity of dimerized HIV-1 protease. Analysis of these data indicated that the FRET-HIV-1 assay system is a reliable tool to evaluate agents for their potential to inhibit protease dimerization.

Inhibition of Protease Dimerization by Non-peptidyl and Peptidyl Compounds—After establishing the validity of the FRET-HIV-1 assay to detect protease dimerization inhibition, we evaluated various newly generated non-peptidyl small molecule agents, including the currently available anti-HIV-1 drugs for their ability to inhibit protease dimerization in a blind manner, where agents examined were identified only under code in conducting the FRET-HIV-1 assay. Six different non-peptidyl small molecule agents (GRL-0036A, GRL-06579A (26), TMC126 (33), GRL-98065 (36), DRV (24), and brecanavir (BCV) (37); M_r, ranging from 547 to 704 (Fig. 3)) were found to disrupt protease

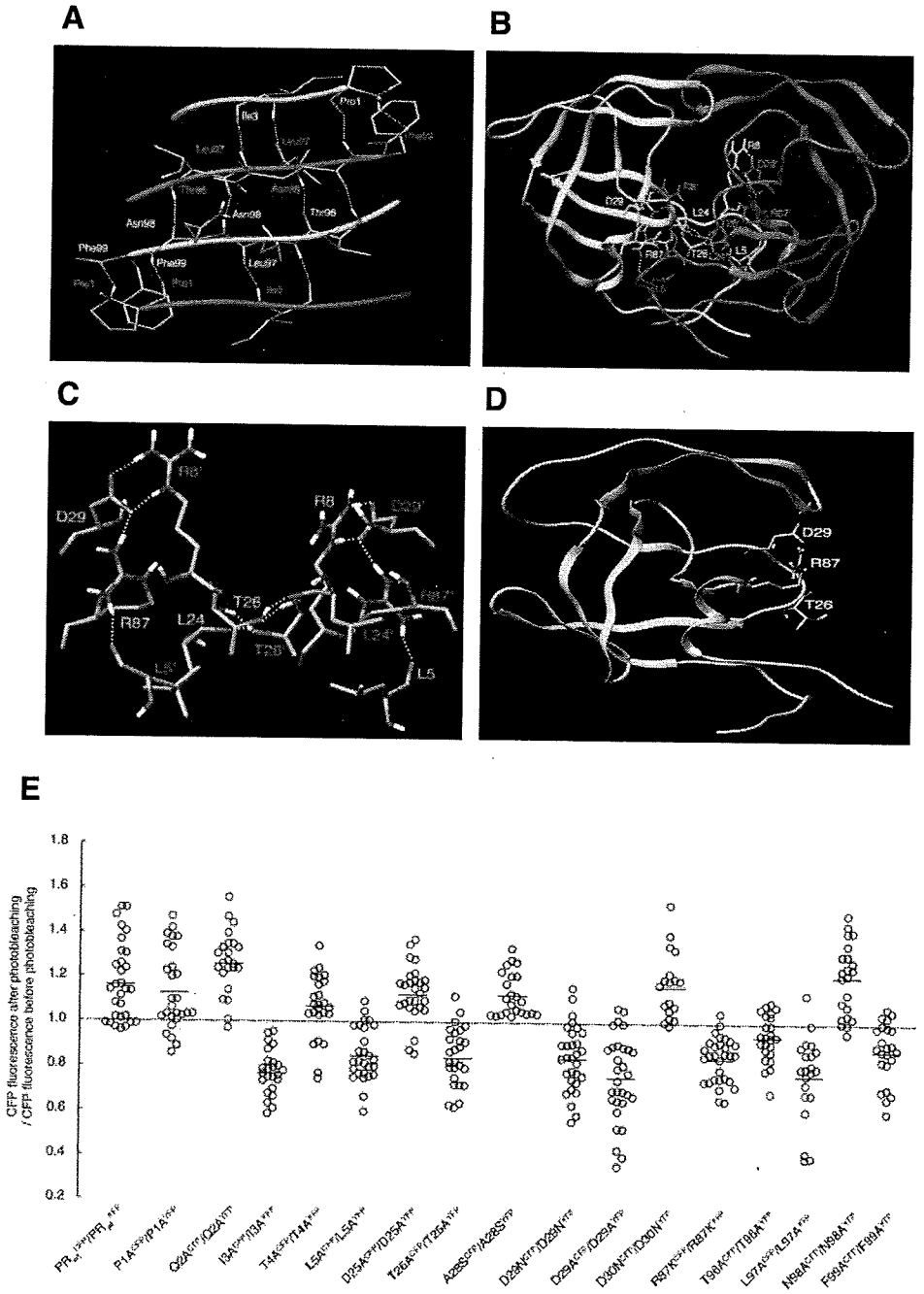

FIGURE 2. **Critical amino acid residues for protease dimerization.** *A*, four antiparallel β-sheets involving the N and C termini of both monomer subunits. Two HIV-1 protease monomer subunits are connected by four antiparallel β-sheets involving the N and C termini of both monomer subunits. It is of note that mature dimerized protease has as many as 12 hydrogen bonds in this N- and C-terminal region, and these interactions seem to be critical for dimer formation. A monomer subunit is shown by the *green ribbon*, and the other monomer subunit is shown by the *red ribbon*. A molecule disrupting these inter-protease hydrogen bond contacts can also disrupt their dimerization. *B* and *C*, intermolecular hydrogen bonds between two HIV-1 protease monomer subunits. The figure shows the intermolecular hydrogen bonds between two protease monomer subunits. The hydrogen bond interactions between protease monomer A (shown as *green ribbon*) and monomer B (shown in *red ribbon*) are Asp-29 to Arg-8′, Arg-87 to Leu-5′, Leu-24 to Thr-26′, and Thr-26 to Thr-26′. The corresponding amino acids of monomer B also form hydrogen bonds with monomer A (*i.e.* Asp-29′ to Arg-8, etc.). Intra-molecular hydrogen bond interaction between Asp-29 and Arg-87 is shown by *white dotted lines*. The residues forming critical intermolecular contacts between two monomer subunits are shown by atom color types (C, *gray*; N, *blue*; O, *red*; and H, *white*). Only polar hydrogens are shown. The residues of chain A are labeled *green*, and those of chain B are labeled *red*. This provides a structural explanation to the FRET experimental data, which show that mutations Leu-5, Asp-29, Thr-26, and Arg-87 prevent formation of a protease dimer. *D*, potential binding sites of the small molecule dimerization inhibitors. The figure shows one of the potential binding sites of the dimerization inhibitors. Asp-29, Arg-87, and Thr-26 are spatially close enough to form binding interactions with the dimerization inhibitor and prevent the other protease monomer from interacting with these residues. *E*, changes in emission intensity ratios upon amino acid substitution. COS7 cells were co-transfected with a pair of HIV-PR^{CFP} and HIV-PR^{YFP} carrying wild-type protease or protease with one amino acid substitution, and CFP$^{A/B}$ ratios were determined. The CFP$^{A/B}$ ratio value for $PR_{WT}{}^{CFP}/PR_{WT}{}^{YFP}$ was 1.17 ± 0.18 (mean ± 1 S.D.); $PR_{P1A}{}^{CFP}/PR_{P1A}{}^{YFP}$, 1.13 ± 0.18; $PR_{Q2A}{}^{CFP}/PR_{Q2A}{}^{YFP}$, 1.26 ± 0.14; $PR_{I3A}{}^{CFP}/PR_{I3A}{}^{YFP}$, 0.77 ± 0.10; $PR_{T4A}{}^{CFP}/PR_{T4A}{}^{YFP}$, 1.07 ± 0.14; $PR_{L5A}{}^{CFP}/PR_{L5A}{}^{YFP}$, 0.85 ± 0.12; $PR_{D25A}{}^{CFP}/PR_{D25A}{}^{YFP}$, 1.13 ± 0.12; $PR_{T26A}{}^{CFP}/PR_{T26A}{}^{YFP}$, 0.84 ± 0.13; $PRA_{28S}{}^{CFP}/PR_{A28S}{}^{YFP}$, 1.13 ± 0.10; $PR_{D29N}{}^{CFP}/PR_{D29N}{}^{YFP}$, 0.84 ± 0.15; $PR_{D29A}{}^{CFP}/PR_{D29A}{}^{YFP}$, 0.76 ± 0.19; $PR_{D30N}{}^{CFP}/PR_{D30N}{}^{YFP}$, 1.17 ± 0.15; $PR_{R87K}{}^{CFP}/PR_{R87K}{}^{YFP}$, 0.84 ± 0.10; $PR_{T96A}{}^{CFP}/PR_{T96A}{}^{YFP}$, 0.94 ± 0.10; $PRL_{97A}{}^{CFP}/PR_{L97A}{}^{YFP}$, 0.77 ± 0.19; $PR_{N98A}{}^{CFP}/PR_{N98A}{}^{YFP}$, 1.21 ± 0.16; and $PR_{F99A}{}^{CFP}/PR_{F99A}{}^{YFP}$, 0.88 ± 0.13. All the experiments were conducted in a blind fashion. The CFP$^{A/B}$ ratio that is >1 signifies a protease dimer, whereas a ratio that is <1 signifies disruption of protease dimerization. Note that the residue (such as Ile-3 or Asp-29) whose mutation resulted in disruption of dimerization had an inter-molecular hydrogen bond contact with the other protease monomer as shown in *A*–*C*. The mean value of the ratios is shown as *bars*.

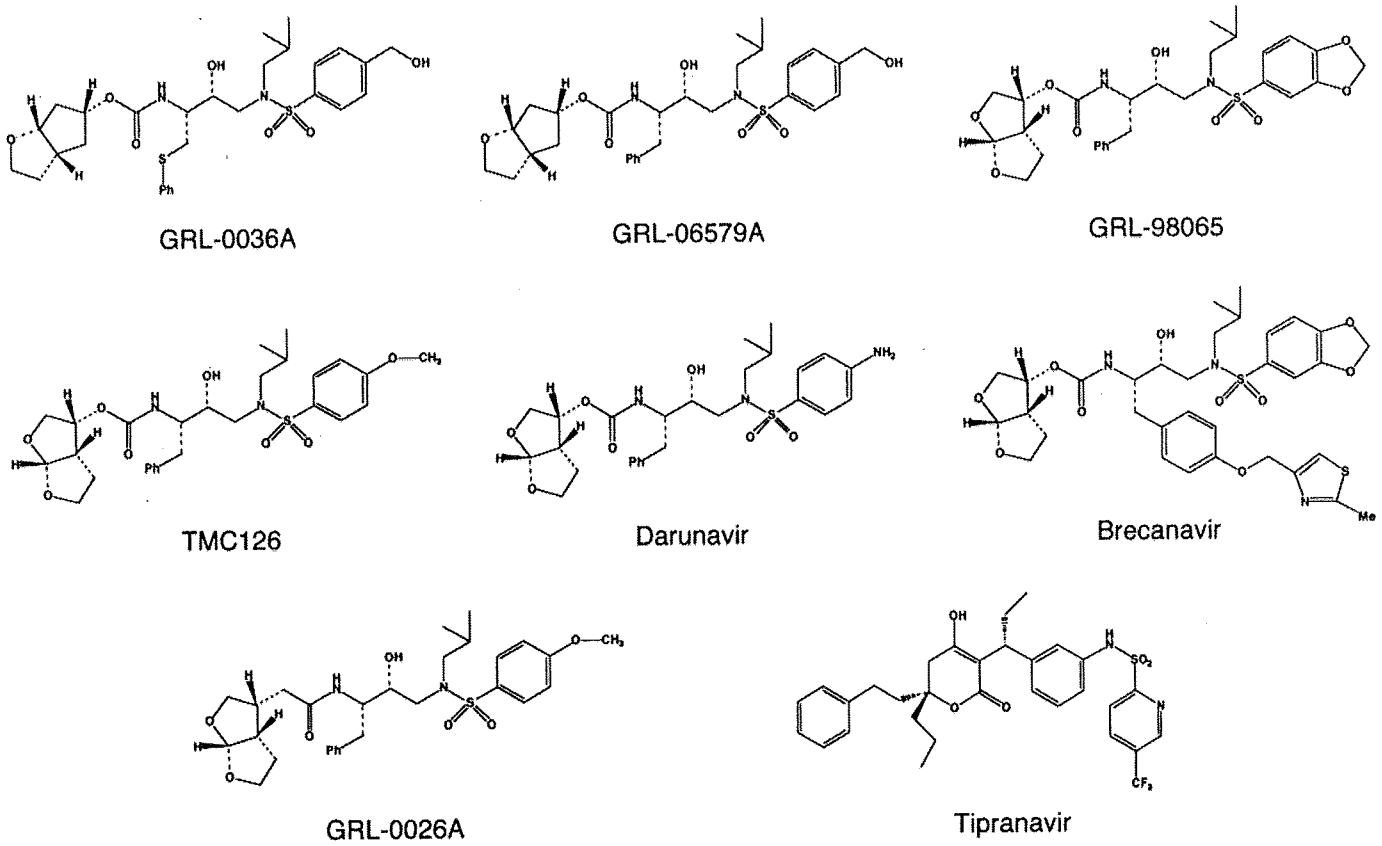

FIGURE 3. **Structures of dimerization inhibitors identified.** Structures of eight dimerization inhibitors are shown. The IC_{50} values for activity against HIV-1 in acute HIV-1 infection assays are shown in Table 1.

dimerization at concentration of 1 μM in the assay (Fig. 4*A*). All of these agents had potent inhibitory activity against HIV-1 protease with K_i values of 29, 3.5, 10, 14, 16, and 6.8 pM, respectively, as examined in the assay previously described (25, 26), and were highly potent against HIV-1_{LAI} in acute HIV-1 infection assays using target $CD4^+$ MT-2 cells (24) with IC_{50} values of 0.0002–0.005 μM (Table 1). In addition to small molecule agents, we examined various peptides in the FRET-HIV-1 assay. A 27-amino acid peptide containing the dimer interface sequences amino acids 1–5 and amino acids 95–99 (P27: PQITLRKKRRQRRRPPQVSFNFATLNF), which blocks HIV-1 infectivity and replication (14), also inhibited protease dimerization as examined in the FRET-HIV-1 expression assay. Another peptide P9 (RKKRRQRRRPPQVSFNF) that lacks the dimer interface sequences and is not active against HIV-1 (14) failed to inhibit protease dimerization in the FRET-HIV-1 assay. These data again corroborated the utility of the assay to evaluate protease dimerization.

To test the robustness and reproducibility of the FRET-HIV-1 assay data, we determined the $CFP^{A/B}$ ratios in a total of 143 COS7 cells transfected with $pPR_{WT}{}^{CFP}$ and $pPR_{WT}{}^{YFP}$ plasmids and cultured in the presence or absence of 1 μM DRV for 3 days on 11 different occasions. In the presence of DRV, only 7 (4.9%) of 143 cells had the ratios of slightly more than 1.0, whereas all the rest (95.1%) had values of <1.0 ($n = 143$; average of 0.73 ± 0.22) (Fig. 4*B*). The $CFP^{A/B}$ ratios determined in the absence of DRV were mostly >1.0 ($n = 172$, average of 1.21 ± 0.17). We next examined whether a dose response in the dimerization inhibition could be seen when the cells were exposed to various concentrations of DRV. As shown in Fig. 4*C*, DRV effectively inhibited protease dimerization at concentrations of 0.1 μM and above, whereas the average $CFP^{A/B}$ ratio was slightly >1.0 at 0.01 μM, and no dimerization inhibition was seen at 0.001 μM. These data show that the inhibition by DRV was roughly dose-responsive up to 0.1 μM. In addition, we examined a TMC126-congener GRL-0026A (Fig. 3) that is substantially less potent than TMC126 against HIV-1 with IC_{50} of 0.48 μM (Table 1), along with TMC126 and BCV for their dose response dimerization inhibition in the FRET-HIV-1 assay and found that the inhibition was similarly dose-responsive (Fig. 4*D*).

None of the FDA-approved Anti-HIV-1 Drugs Except TPV Blocks Dimerization—We asked whether other currently approved PIs blocked protease dimerization in the FRET-HIV-1 assay. None of the seven PIs (saquinavir, nelfinavir, amprenavir, indinavir, ritonavir, lopinavir, and atazanavir) inhibited protease dimerization at 1 μM concentration, whereas the control DRV clearly inhibited the dimerization as shown in Fig. 4*E*. Considering that DRV is generally more potent against HIV-1 *in vitro* than most currently existing PIs (24), four PIs (saquinavir, amprenavir, nelfinavir, and atazanavir) were examined in the FRET-HIV-1 assay at a higher concentration, 10 μM, however, none of these four PIs inhibited protease dimerization (Fig. 4*F*). Interestingly, TPV, which has been shown to provide more favorable virological and immunological responses in patients who have received extensive previous antiretroviral treatment than an optimized background regimen when

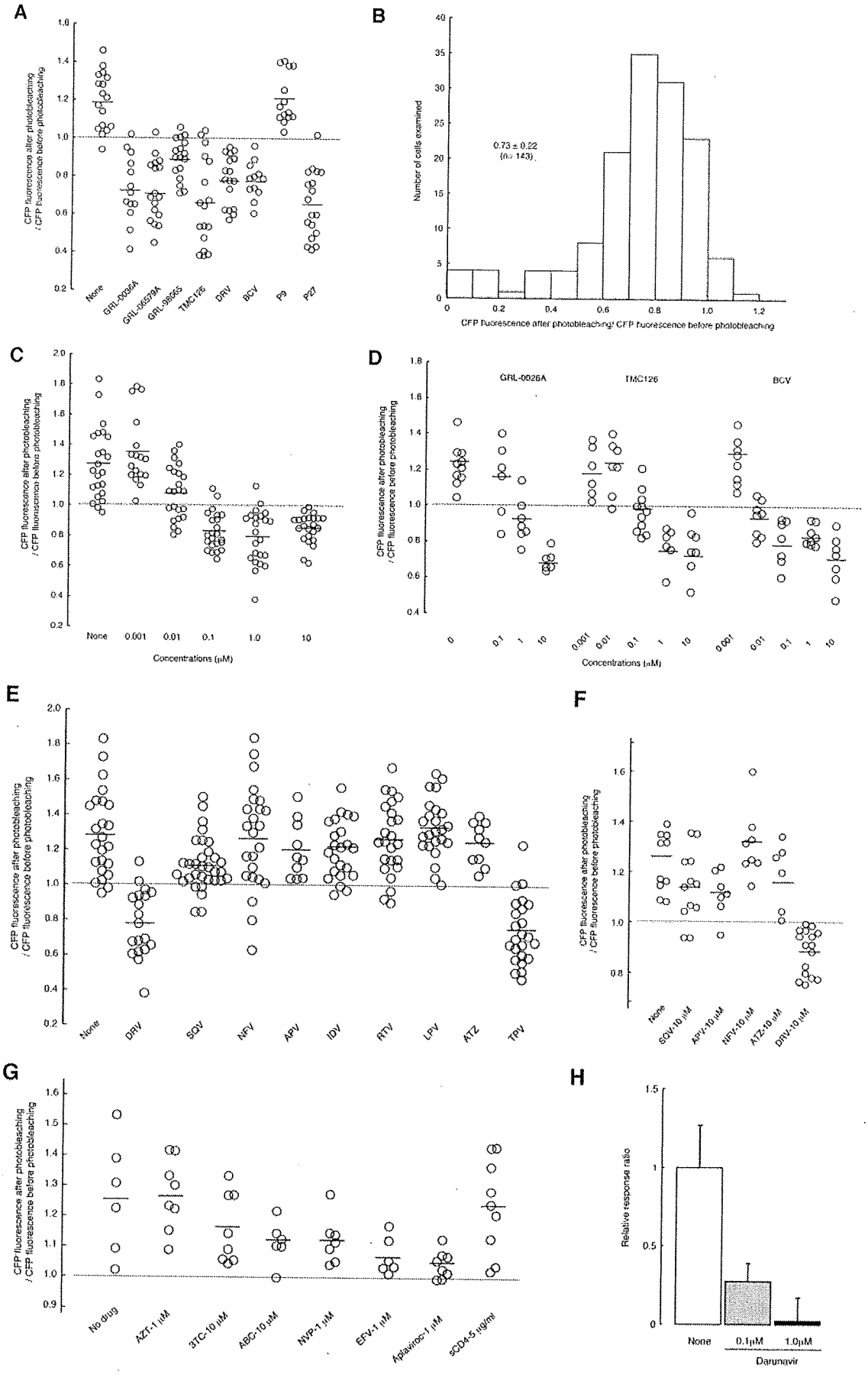
A
CFP fluorescence after photobleaching / CFP fluorescence before photobleaching
None
GRL-0026A
GRL-06579A
GRL-98065
TMC126
DRV
BCV
P9
PZ7
B
Number of cells examined
0.73 ± 0.22
(n = 143)
CFP fluorescence after photobleaching/ CFP fluorescence before photobleaching
C
CFP fluorescence after photobleaching / CFP fluorescence before photobleaching
None
0.001
0.01
0.1
1.0
10
Concentrations (μM)
D
GRL-0026A
TMC126
BCV
CFP fluorescence after photobleaching / CFP fluorescence before photobleaching
Concentrations (μM)
E
CFP fluorescence after photobleaching / CFP fluorescence before photobleaching
None
DRV
SQV
NFV
APV
IDV
RTV
LPV
ATZ
TPV
F
CFP fluorescence after photobleaching / CFP fluorescence before photobleaching
None
SQV-10 μM
APV-10 μM
NFV-10 μM
ATZ-10 μM
DRV-10 μM
G
CFP fluorescence after photobleaching / CFP fluorescence before photobleaching
No drug
AZT-1 μM
3TC-10 μM
ABC-10 μM
NVP-1 μM
EFV-1 μM
Aptavirоc-1 μM
sCD4-5 μg/ml
H
Relative response ratio
None
0.1μM
1.0μM
Darunavir